Bioorganic & Medicinal Chemistry 18 (2010) 2375–2387

Contents lists available at ScienceDirect

Bioorganic & Medicinal Chemistry

journal homepage: www.elsevier.com/locate/bmc

Pyrazolone-fused combretastatins and their precursors: synthesis, cytotoxicity, antitubulin activity and molecular modeling studies

Bojan Burja [a,†], Tamara Čimbora-Zovko [b,†], Sanja Tomić [c], Tihana Jelušić [b], Marijan Kočevar [a], Slovenko Polanc [a,*], Maja Osmak [b,*]

[a] Faculty of Chemistry and Chemical Technology, University of Ljubljana, Aškerčeva 5, SI-1000 Ljubljana, Slovenia
[b] Division of Molecular Biology, Ruđer Bošković Institute, Bijenička cesta 54, HR-10000 Zagreb, Croatia
[c] Division of Physical Chemistry, Ruđer Bošković Institute, Bijenička cesta 54, HR-10000 Zagreb, Croatia

ARTICLE INFO

Article history:
Received 21 January 2010
Revised 26 February 2010
Accepted 4 March 2010
Available online 10 March 2010

Keywords:
Combretastatin CA-4 derivatives
Cytotoxicity
Tubulin
Molecular modeling

ABSTRACT

A series of pyrazolone-fused combretastatins and precursors were synthesized and their cytotoxicity as well as antitubulin potential was evaluated. The hydrazide **9f** and the pyrazolone-fused combretastatins **12a**, **12b** and **12c** were highly cytotoxic against various tumor cell lines including cisplatin resistant cells. The same compounds were also the best inhibitors of tubulin polymerization. Molecular modeling results showed that they bind the colchicine binding site at the tubulin heterodimer. The hydrazide **9f** arrested HeLa cells in the G2/M phase of the cell cycle and strongly affected cell shape and microtubule network.

1. Introduction

Pyrazoles play an important role among biologically active compounds.[1] Typical pyrazole derivatives are pyrazol-3-ones ('pyrazolones') whose syntheses, reactivity and numerous applications are well-documented.[2–4] Pyrazolone derivatives were examined for growth-inhibitory properties in several human cancer cells.[5] Some of them are effective inhibitors of heptosyltransferase WaaC,[6] others inhibit accumulation of the abnormal protease-resistant form of prion protein (PrP-res).[7] We considered the pyrazolone ring as a part of the tricyclic molecules that may be used as potential inhibitors of tubulin polymerization. Namely, the agents acting on microtubules have played a central role in the treatment of diverse human cancers over the past decade.[8] Recently reported compounds targeting the colchicine-binding domain can serve as agents that rapidly depolymerize microtubules of newly formed vasculatures and block the blood supply to tumors.[9]

Many small molecules of various types are known to bind at the colchicine site of tubulin.[10] Among them is also combretastatin A-4 (**1a**, Fig. 1) as one of the most potent antimitotic agents.[11] This compound, a natural product isolated from the South African tree *Combretum caffrum*, is highly cytotoxic against a variety of human cancer cells, including drug-resistant cell lines.[12] Combretastatin A-4 binds at or near the colchicine binding site and inhibits tubulin polymerization resulting in cell death.[11] The molecule induces irreversible vascular shutdown within solid tumors while leaving normal vasculature intact.[13] A great interest in such molecules is reflected in the fact that two combretastatin A-4 analogues (**1b**, **1c**) and one combretastatin A-1 derivative (**2**) are currently in clinical trials (Fig. 1).[14,15]

The major disadvantages of combretastatin A-4 as a drug candidate are low water solubility and low bioavailability. However, the encouraging antivascular and anticancer activity of CA-4 has stimulated the synthesis and evaluation of a large number of CA-4 analogues.[16–20] Their structure–activity relationship (SAR) has shown that combretastatin A-4 appears distinct in three different parts: (a) the 3,4,5-trimethoxyphenyl moiety (A-ring), which influences cytotoxicity, (b) the double bond that affects both the cytotoxicity and the tubulin binding, and (c) the B-ring (phenol) which influences binding to tubulin.[11] Since the isomerization from the *cis* to the less active *trans* form is the weakness of combretastatin A-4 as a potential anti-cancer drug, we thought to retain its effectiveness by locking the appropriate stereochemistry of the two rings by fusion of the combretastatin C=C double bond with a five-membered or a six-membered ring. Heterocyclic rings[21–24] and cyclopent-2-en-1-one[25] were considered to address this issue. However, before the design of our novel pyrazolone derivatives that might exhibit antiproliferative and antitubulin effects, two examples (**3** and **4**, Fig. 1) have already been described possessing adjacent aryl groups

* Corresponding authors. Tel.: +386 1 24 19 236; fax: +386 1 24 19 271 (S.P.); tel.: +385 1 4560 939; fax: +385 1 4561 177 (M.O.).
E-mail addresses: slovenko.polanc@fkkt.uni-lj.si (S. Polanc), osmak@irb.hr (M. Osmak).
† Both authors contributed equally to the manuscript.

0968-0896/$ - see front matter © 2010 Elsevier Ltd. All rights reserved.
doi:10.1016/j.bmc.2010.03.006

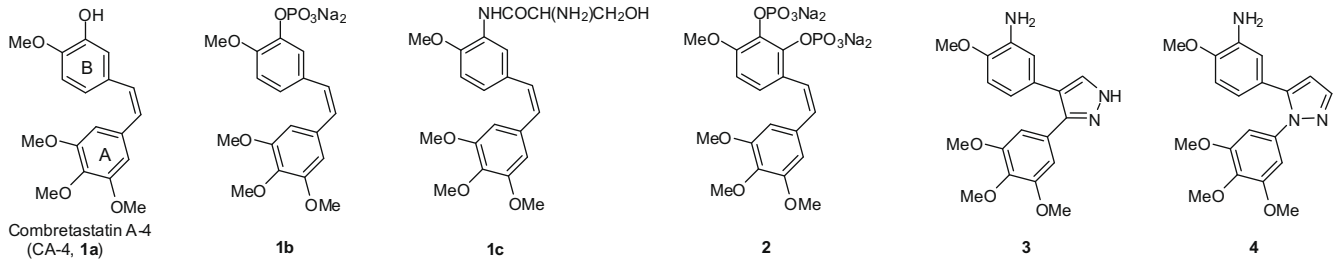

Figure 1. Combretastatin A-4 and analogous compounds.

either at the positions 2,3-[26] or 1,5-[21] of the pyrazole ring. It should be added that some 3,5-disubstituted pyrazoles[27] and 3,5-disubstituted pyrazolines[28] have also been studied, but they are structurally different from our CA-4 derivatives having C–C═C linkage rather than C–C or C–N connection between the two aryl groups. To the best of our knowledge there are no reports in the literature on combretastatins having Ar^1 and Ar^2 groups at the positions 4 and 5 of the pyrazolone ring.

Our new compounds were designed to test structure–activity relationship arising from the number and position of the methoxy groups in A or B rings, the introduction of the fluorine atom, the replacement of the entire aromatic ring, or the interchange of rings A and B. Here we report the synthesis, cytotoxic activity and antitubulin effect for the pyrazolone-fused combretastatins and their precursors. For the most active compound, **9f**, we examined its cytotoxicity on a variety of cancer cell lines, and explored its influence on the cell cycle, as well as on the cell morphology and microtubule network. Finally, molecular modeling studies were performed with the colchicine binding site of α,β-tubulin in an attempt to explain the biological effects.

2. Results and discussion

2.1. Synthesis

We recently disclosed a new and general route to pyrazol-3-ones starting from commercially available propenoic acids.[29] This approach was mainly demonstrated on 3-substituted propenoic acids but two examples of the application on 2,3-disubstituted propenoic acids were also described. Inspired by these results, we envisaged the synthesis of pyrazolone-fused combretastatins. The preparation of the first target is shown in Scheme 1.

Thus, the Perkin reaction between 3-hydroxy-4-methoxybenzaldehyde (**5a**) and 3,4,5-trimethoxyphenylacetic acid (**6a**) in acetic anhydride using triethylamine as a base led to 2,3-diarylpropenoic acid **7a** as the final product. The next step required a protection of the phenol, which was done by the acetylation to obtain **7a′**. Then, the acid **7a′** was transformed to the acid chloride **8a** and its further reaction with methyl carbazate gave the disubstituted hydrazide **9a** that was then oxidized to the corresponding diazene **10a**. Although the latter compound may be treated with $ZrCl_4$ at room temperature to yield the combretastatin derivative **11a** we also found that a Lewis acid was not required to perform the cyclization of the diazene. Namely, a ring-closure to **11a** takes place also on heating the diazene in dichloromethane under reflux (see, general procedure). The final step was a hydrolysis of the ester functionality and subsequent decarboxylation, accompanied by the deacetylation of the protected phenolic group that resulted in the formation of the desired pyrazolone-fused combretastatin **12a**.

Following the described reaction scheme several other compounds were prepared employing the appropriate aromatic aldehydes and arylacetic acids. The structures of analogous products, namely, **7b**–**7i**, **9b**–**9i**, **11b**–**11i**, and **12b**–**12i**, are depicted in Figure 2. In these cases there was no functional group present in acids **7** that would have required the appropriate protection.

It is worth mentioning that the 3,4,5-trimethoxyphenyl group in most of the above compounds appears at the same position as in **7a**–**12a** (i.e., Ar^1). On the other side, in analogues **h**, the 3,4,5-trimethoxyphenyl moiety serves as Ar^2 while in the case of the products **i** the 2,4,5-trimethoxyphenyl group is attached at this position. We decided to evaluate not only the biological activity of pyrazolone-fused combretastatins **12** but also their precursors **9** and **11** as all of them possess the desired stereochemistry.

2.2. Biological evaluation

Cytotoxic effects of pyrazolone-fused combretastatins, their precursors, and the reference compound (CA-4) were evaluated on human cervical carcinoma HeLa cells (Table 1). The screening revealed that the precursor of the combretastatin derivative, a disubstituted hydrazide **9a** was highly cytotoxic. The activity against the same cells increased when employing pyrazolone-fused compound **11a** as well as in the case of **12a**.

Variations of the aryl groups of **9a** demonstrated their high impact on cytotoxicity of the modified compounds. An introduction of 2-naphthyl substituent as Ar^2 (see, **9f**) resulted in 10 times increase of the antiproliferative activity comparing to **9a**. Thus, the hydrazide **9f** exhibited the highest antiproliferative activity of all examined new molecules. Having 1-naphthyl as the substituent Ar^2, the compound **9e** was less cytotoxic than **9a**. Furthermore, variations of substituents within the Ar^2 moiety of **9a** led either to the reduced activity (**9b**, **9c**) or made a new compound almost inactive (see, **9d** and **9g**). On the other hand, if Ar^1 was replaced with 3,4-dimethoxyphenyl group, the new compound had very low antiproliferative activity (**9h**), or was not active at all (**9i**). Identical modifications of the structures of **11a** and **12a**, as described above for **9a**, reflect similar trends in activity against HeLa cells (except for **11f** and **12f).** This is evident comparing **11b**–**11i** versus **11a** and **12b**–**12i** versus **12a**, respectively. The cytotoxic effect of **11f** compared to **11a** was reduced, while that of **12f** was increased compared to **12a**, but these differences in activities were modest. The lowest influence of the modifications in Ar^2 moiety with 3,4,5-trimethoxyphenyl as Ar^1 was detected for pyrazolone-fused combretastatins **12a**, **12b** and **12c**.

The structural resemblance of pyrazolone-fused combretastatins and their precursors with CA-4 encouraged us to investigate the ability of these compounds to effectively inhibit tubulin polymerization. Namely, some recent reports suggest that nonlinear relationship between proliferation inhibition and the effect on tubulin polymerization of combretastatin analogues may occur, where highly cytotoxic compounds are not necessarily potent inhibitors of tubulin polymerization and vice versa.[11,20,30] In initial screening, we evaluated the inhibition of tubulin polymerization of new compounds at a single concentration of 20 μM (Table 1).

The analysis of correlation for cytotoxic and antitubulin potential of pyrazolone-fused combretastatins and their precursors

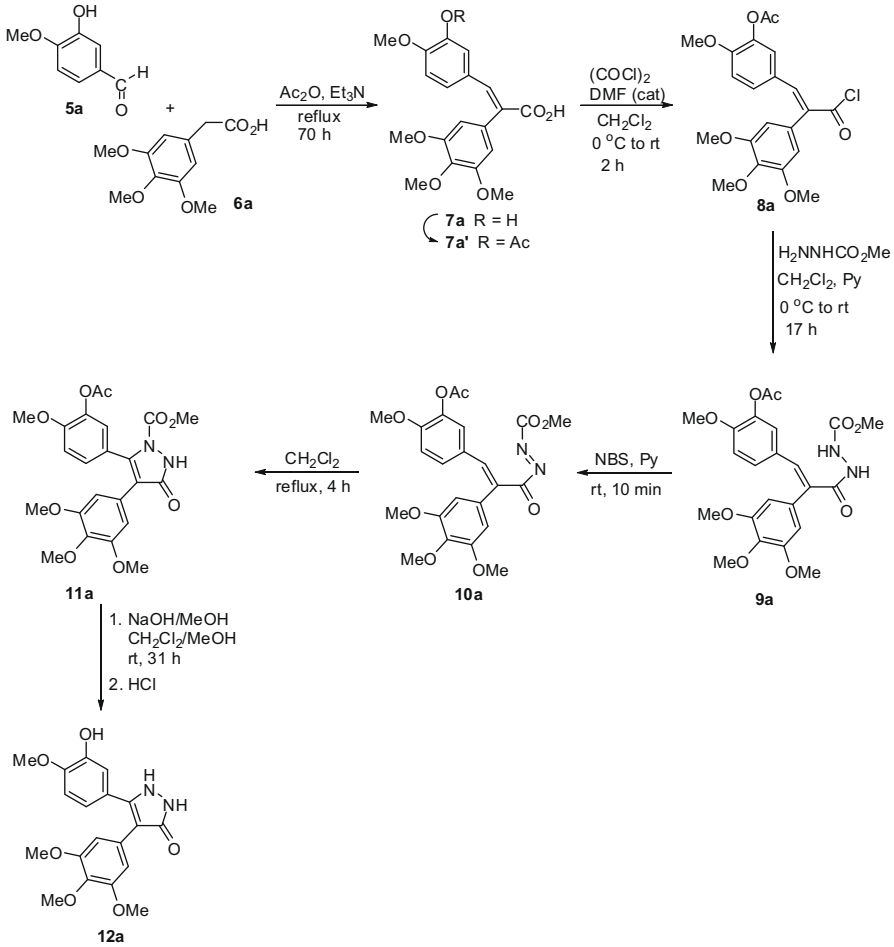

Scheme 1. Synthesis of the first pyrazolone-fused combretastatin A-4 derivative and its precursors.

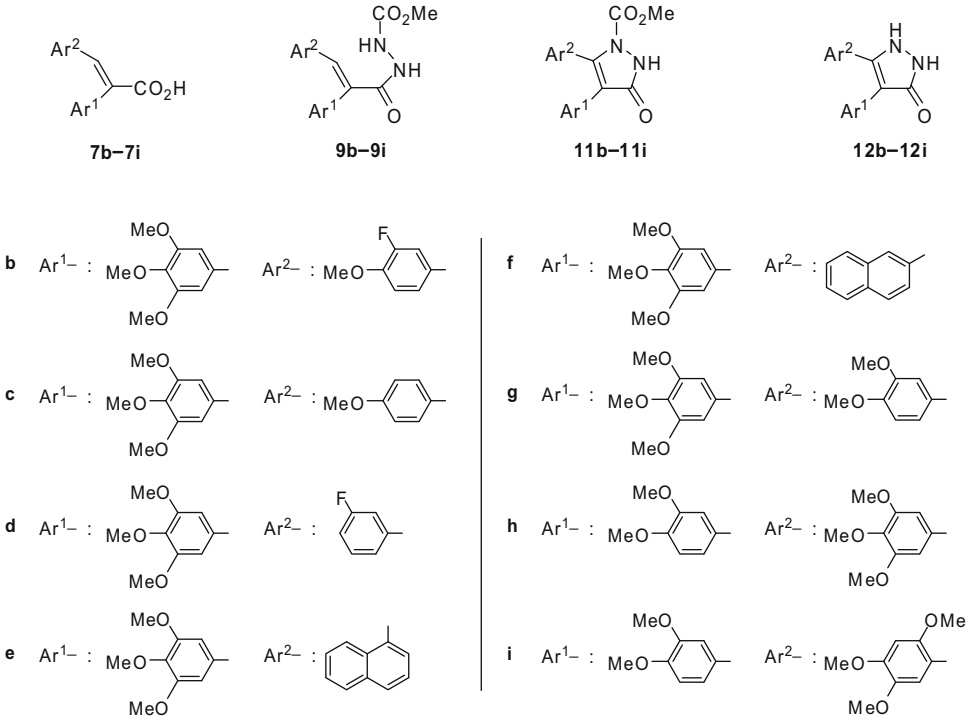

Figure 2. Structures of the pyrazolone-fused combretastatins and their precursors.

Table 1
Cytotoxicity of studied compounds against HeLa cells and their inhibition of tubulin polymerization

Compound	IC_{50}[a] (μM)	%TPI[b]
9a	0.498 ± 0.006	25
9b	0.667 ± 0.072	66
9c	1.31 ± 0.19	26
9d	>50	10
9e	1.30 ± 0.15	55
9f	0.048 ± 0.001	97
9g	>50	0
9h	>50	0
9i	NA	0
11a	0.337 ± 0.107	0
11b	1.72 ± 0.59	9
11c	0.959 ± 0.151	0
11d	NA	1
11e	>50	7
11f	0.523 ± 0.036	3
11g	36.3 ± 2.2	3
11h	NA	0
11i	NA	2
12a	0.176 ± 0.011	99
12b	0.158 ± 0.024	100
12c	0.152 ± 0.020	100
12d	>50	0
12e	>50	0
12f	0.114 ± 0.006	98
12g	5.27 ± 1.53	31
12h	>50	4
12i	>50	0
CA-4	0.002 ± 0.0001	89

[a] IC_{50} is the concentration of the test compound inducing 50% cell growth inhibition after 72 h incubation; NA: not active. Values representative mean ± SD from at least three experiments.
[b] Tubulin polymerization inhibitory activity is expressed as the percentage of polymerization of the sample with respect to the control (% TPI) at a single dose of 20 μM. Values representative of two experiments.

shows very interesting data (Table 1). In the group of disubstituted hydrazides (compounds **9**), the introduction of 2-naphthyl substituent as Ar^2 which strongly increased the cytotoxicity of **9f**, increased also its antitubulin potential. Other alterations in Ar^2 which reduced the cytotoxic activity of **9b**, **9c** and **9e**, reduced also their capacity to inhibit tubulin polymerization, but the relationship between cytotoxicity and antitubulin effect was not linear (e.g., very cytotoxic **9c** only modestly inhibits tubulin polymerization). In addition, the alterations in Ar^1 or Ar^2 that strongly reduce or cause the complete loss of the antiproliferative activity (compounds **9d**, **9g**, **9h** and **9i**) are associated with a negligible antitubulin potential.

The cyclization of hydrazides **9** into N-1 protected pyrazolone-fused combretastatins **11** led to the complete loss of any antitubulin activity, irrespective of the alterations in Ar^1 or Ar^2 functionalities. These results suggested that the methoxycarbonyl group totally blocked their antitubulin potential. This was indeed confirmed by studies performed on N-1 deprotected pyrazolones **12** where a good correlation between cytotoxicity and antitubulin activity was observed.

Based on the tubulin polymerization inhibitory activity determined after a single concentration of pyrazolone-fused combretastatins and their precursors (Table 1), we selected those that most efficiently inhibited tubulin polymerization to determine their IC_{50}, that is, a concentration of the compound required to inhibit 50% of the rate of microtubule assembly. However, the IC_{50} values for inhibition of tubulin polymerization were not much different from IC_{50} obtained for CA-4: 1.7 μM for **12a**, 2.6 μM for **12c**, 1.9 μM for **12f**, 2.7 μM for **9f** and 2.0 μM for CA-4.

As the compounds **9f**, **12a**, **12b** and **12c** were highly cytotoxic and effectively inhibited tubulin polymerization, we determined their cytotoxicity on various tumor cell lines (Table 2).

The screening results revealed that the selected compounds strongly inhibited the growth of all examined tumor cell lines, and this effect depended on the cell type. Human cervical carcinoma HeLa cells were more sensitive toward our compounds than any other cancer cells and were used in our further studies. The cell-type dependent difference in the cell sensitivity to selected compounds ranged from 4 (**9f**) to 21 times (**12b**). It should be pointed out that cisplatin resistant CK2 cells were significantly more sensitive to **12a** and **12b** than parental HEp-2 cells. Furthermore, invasive urinary bladder carcinoma T-24 cells were more sensitive to **12a**, **12b** and **12c** than non-invasive urinary bladder carcinoma RT-112 cells. The latter cells turned out to be the most resistant among the examined cell lines. Again, CA-4 itself was more cytotoxic than any other compound on the same cancer cell line.

For the most active compound, **9f**, we examined its effect on the cell cycle progression on HeLa cells. This effect was investigated by flow cytometry after 24 h of treatment with various concentrations of the selected compound, and compared to the effect of CA-4 (Table 3). The lowest concentration of **9f** (0.02 μM) gave no alteration in the distribution of cells through the cell cycle. The 10 times higher concentration (0.2 μM) arrested the majority of cells in G2/M phase of the cell cycle. However, if the same concentrations of CA-4 were used, already the lowest concentration (0.02 μM) almost completely arrested cells in G2/M phase of the cell cycle. The arrest in G2/M phase was accompanied with an increase of sub-G_1 cells, consistent with the occurrence of apoptotic DNA fragmentation. Thus, both compounds induced similar perturbation in the cell cycle of HeLa cells.

To support our results that selected compounds inhibit polymerization of tubulin, we evaluated their capacity to alter the microtubule network by tubulin immunostaining, comparing it to that of CA-4 (Fig. 3). Human cervical carcinoma HeLa cells were treated with different concentrations (0.02, 0.2 and 2.2 μM) of these compounds for 24 h. As expected, even the lowest concentration of CA-4 completely disrupted microtubule structure compared to untreated controls (Fig. 3), while the same concentration of **9f**

Table 2
Antiproliferative activity of selected pyrazolone-fused combretastatins and their precursors towards various cancer cell lines (IC_{50}, μM ± SD)

Compd/cells	**9f**	**12a**	**12b**	**12c**	CA-4
HeLa	0.048 ± 0.001	0.176 ± 0.011	0.158 ± 0.024	0.152 ± 0.020	0.002 ± 0.0001
HEp-2	0.054 ± 0.001	1.142 ± 0.138	1.179 ± 0.236	0.529 ± 0.081	0.0055 ± 0.0017
CK2	0.051 ± 0.001	0.709 ± 0.120	0.684 ± 0.238	0.615 ± 0.277	0.0052 ± 0.0011
RT-112	0.1961 ± 0.0934	2.083 ± 0.074	3.319 ± 1.932	1.888 ± 0.116	0.0216 ± 0.00381
T-24	0.1848 ± 0.061	0.619 ± 0.075	1.154 ± 0.589	1.156 ± 0.662	0.0087 ± 0.0006
MIA PaCa-2	0.127 ± 0.072	0.462 ± 0.078	0.556 ± 0.059	0.575 ± 0.025	0.0072 ± 0.0011
SW620	0.0743 ± 0.0032	0.543 ± 0.175	0.487 ± 0.188	0.455 ± 0.176	0.023 ± 0.0005

IC_{50} is the concentration of a compound inducing 50% cell growth inhibition after 72 h incubation. HeLa = cervical carcinoma cells, HEp-2 = laryngeal carcinoma cells, CK2 = cisplatin-resistant HEp-2 subline, RT-112 = urinary bladder carcinoma cells, T-24 = urinary bladder carcinoma cells, MIA PaCa-2 = pancreatic carcinoma cells, SW620 = colorectal carcinoma cells.

Table 3
Effects of **9f** and CA-4 on cell cycle of HeLa cells

Concd (μM)	CA-4				**9f**			
	$G_{0/1}$ (%)	S (%)	G_2/M (%)	Apo (%)	$G_{0/1}$ (%)	S (%)	G_2/M (%)	Apo (%)
0	58.7	29.3	12.1	5.7	58.7	29.3	12.1	5.7
0.02	1.8	8.2	90.0	20.7	60.2	28.3	11.5	6.9
0.2	1.2	8.6	90.2	16.4	2.7	10.8	86.6	21.1
2.2	1.6	7.9	90.5	15.4	1.2	7.7	91.1	21.4

HeLa cells were treated for 24 h with **9f** and CA-4, stained with propidium iodide and analyzed by flow cytometry. Cell cycle distribution was assessed as described in Section 4.

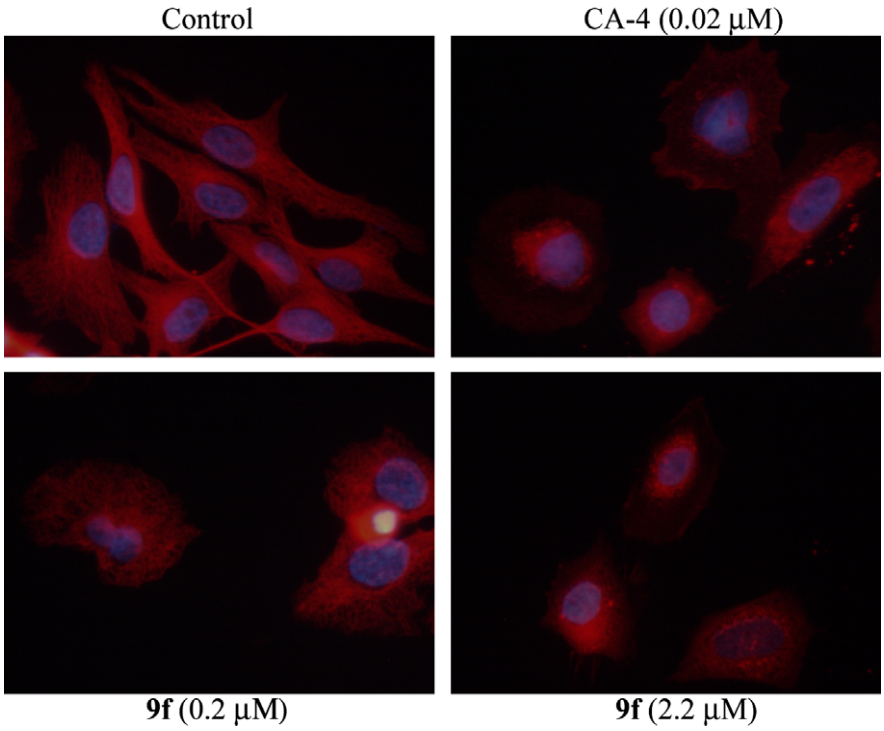

Figure 3. Effect of the hydrazide **9f** and CA-4 on microtubule network of HeLa cells. HeLa cells, treated for 24 h with the indicated concentrations of **9f** or CA-4, were stained with antibody against β-tubulin (red) and DAPI (blue).

had no effect on microtubule network (data not shown). With ten times higher concentration of **9f** a partial disruption of microtubules was seen, whereas with the highest concentration disruption was complete and comparable to the one observed with CA-4 (Fig. 3). Similar effects on microtubule network were determined for **12a**, **12b**, **12c** and **12f** (data not shown). Thus, selected compounds strongly affected the cell shape and microtubule arrangement in a manner comparable to CA-4.

2.3. Molecular modeling

To explain marked difference between cytotoxicity and antitubulin potential of the compounds **9f**, **11a**, **11f**, **11g**, **12a**, **12b**, **12c** and **12f**, we evaluated in silico their binding to the colchicine binding site at the tubulin heterodimer. The ligands were docked into the colchicine binding site, solvated and subjected to molecular dynamics (MD) simulations. During 200 ps of MD simulations ligands nicely accommodated within the protein binding site. Terminal rings of all ligands occupy the same cavities making similar interactions with the protein (Supplementary data, Fig. SD1). However, the interactions between the ligand and protein significantly differ mainly due to different linkers. For example interaction with GTP is the largest in the complex with **9f**, followed by **11a** and **11f**. During MD simulations water molecules enter the binding place and mediate interactions between the bound ligand and protein, see for example, Figure 4.

In the final conformation CA-4 interacts via strong H-bond (O···NH) with Valα181 backbone, and Cysβ241 side chain, with Alaα180 and Lysβ352 it interacts by the weak CH···O hydrogen bonds, with Leuβ255 by CH···π interaction, and with Alaβ316 and Valα181 side chains by hydrophobic, van der Waals interactions. It is interesting that orientation of the Lysβ352 side chain in the CA-4 complex with tubulin differs from its orientations in the other complexes (Supplementary data, Fig. SD2). The final **9f** conformation interacts by strong NH···O H-bonds with the Asnα101 side chain and with the Alaβ250 back bone (Fig. 5). Furthermore, **9f** interacts with Cysβ241 and Leuβ248 by strong electrostatic, CH···O, interactions, with the Alaβ250 and Thrα179 side chains by weak CH···O hydrogen bonds, with Alaβ250 by CH···π interaction and with Leuβ252, Leuβ255 and Alaα180 side chains by hydrophobic, van der Waals interactions.

Compounds **11f** and **12f** occupy an almost identical binding space as **9f**, but their interactions with Alaβ250, and GTP are weaker. Pyrazolone-fused combretastatin **11a** strongly interacts, similarly as CA4, **9f** and **11f**, with Asnβ258 and Lysβ352. They have multiple CH···O and CH···π interactions with Alaβ250; in comparison with other ligands its interaction with Cysβ241 is stronger. A pyrazolone derivative **11g** interacts with Ileβ378 Leuβ255,

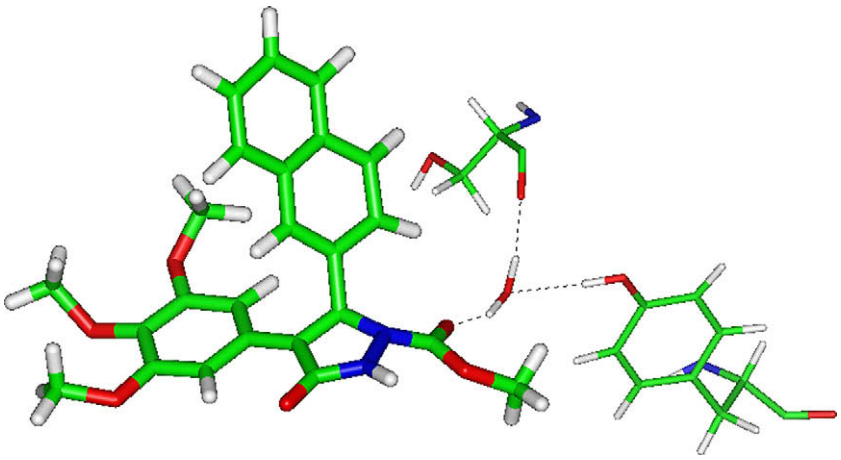

Figure 4. Water mediated hydrogen bond between **11f**, Serα178 and Tyrα224.

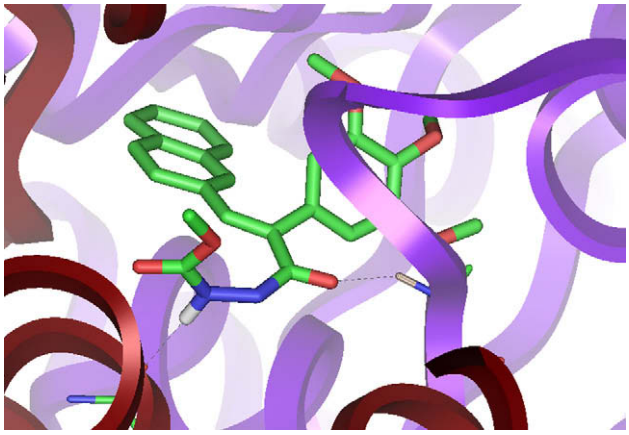

Figure 5. The compound **9f** binds to the tubulin at the colchicine binding site. Hydrogen bonds with Asnα101 and Alaβ250 back bone are displayed.

Thrβ353, and Valα181. Furthermore, **12a** interacts with Valβ315 by a CH···O H-bond (see Fig. 6), with the side chain of Cysβ241 it interacts by strong electrostatic CH···π interaction, with Metβ259 and Asnβ258 side chains by CH···O and CH···N electrostatic interactions, respectively. With Alaβ317 back bone it has weak electrostatic NH···O interactions, and with Lysβ254, Leuβ255, Thrβ314 and Valα181 side chains, and Lysβ352 back bone **12a** interacts by hydrophobic, van der Waals interactions. The side chain of Cysβ241 in its complex with tubulin has different orientations than in the other complexes, for example, in those with CA-4 and **9f**. When looking into the position of **12c** and CA-4 in the tubulin binding site, it can be seen that they occupy a similar space in the binding pocket. The main difference is a lack of the CH···O H-bond with Valα181 and significant weakening of the interaction with Lysβ352. Instead, **12c** is bonded by CH···O hydrogen bond to the Alaβ250. The study also showed that **12b** is similarly as **12c** stabilized by the CH(Alaβ250)···O hydrogen bond and lacks the CH(Valα181)···O H-bond.

The main reason for a significantly lower activity of these compounds in respect to CA-4 might be their considerably lower lipophilicity (Table 4). However, there are also differences in interaction between alpha and beta subunits which should not be neglected when considering their influence on tubulin polymerization.

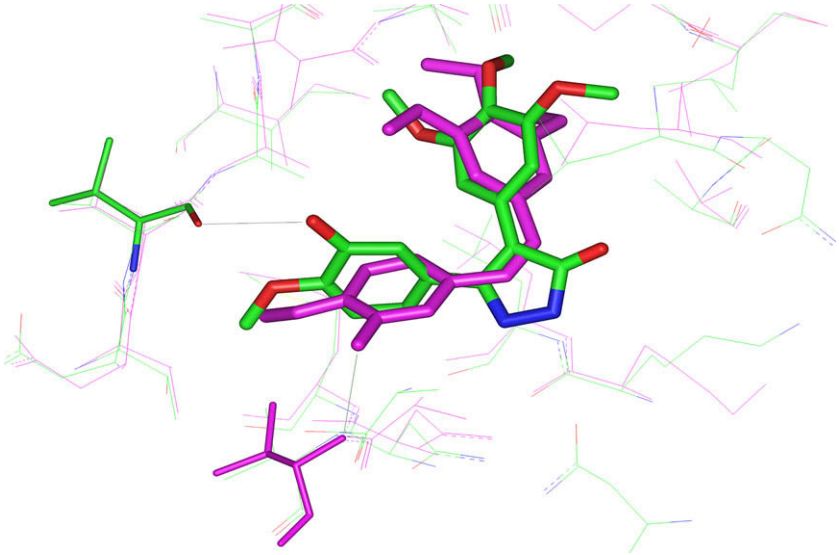

Figure 6. Overlap of the CA-4 (violet) and **12a** (colored according to the atom type) binding modes. The hydrogen bond between **12a** and Valβ315 and between CA-4 and Valα181 are shown as thin gray lines.

Table 4
Lipophilicity (Log *P*) and solubility (Log *S*) of the selected compounds calculated by ALOGPS 2.1[31]

Compound	Log *P*	Log *S*
9f	3.28	−5.73
11a	2.20	−4.59
11f	3.31	−5.09
11g	2.58	−4.20
12a	1.49	−3.35
12b	1.57	−3.85
12c	2.23	−4.14
12f	3.25	−4.89
CA-4	3.32	−4.51

According to the Log *P* and Log *S* data calculated by ALOGPS 2.1, the substrates **9f**, **11f**, **12f** and CA-4 are more lipophilic than the other analyzed substrates (Table 4). This means that their transport through the cell membrane is easier and consequently their probability to bind to tubulin is increased, but also a change of the electrostatic component of the free energy of desolvation, due to the complex formation, is improved for these compounds compared to the other substrates shown in Table 4. However, the measured binding affinity could not be explained only by the substrate hydrophilicity. From the calculated interaction energies between polar and charged probes and the substrates, only very limited conclusions could be derived. From all selected compounds, **11g** has the weakest interaction with O-probe and this might partly explain its low binding affinity.

Apparently, the measured biological data can not be rationalized using an isolated theoretical approach. It seems that various computational tools need to be used: the protein docking and the molecular dynamic study results might be more revealing by taking into account the calculated ADME (Absorption, Distribution, Metabolism and Excretion) properties.[32]

3. Conclusions

The aim of the present study was to lock the moieties Ar^1 and Ar^2 of combretastatin-like compounds in the active *cis* position by constructing the pyrazolone ring that includes the C=C bond and to test the structure–activity relationship arising from variations in the number and the position of methoxy groups on aromatic rings, by an introduction of the fluorine atom into the molecule or by the interchange of Ar^1 functionality with Ar^2.

Regarding cytotoxicity, the ring-closure of the corresponding diazenes to the pyrazolone-fused combretastatins **11** resulted in drastically reduced cytotoxicity comparing to CA-4. However, the hydrazide **9f** having a 2-naphthyl substituent for the group Ar^2, exhibited much higher cytotoxicity than the compounds of type **11**. Contrary, other variations of the aryl groups (structures **d**, **g**, **h** and **i**) inhibited or even blocked the antiproliferative activity of the new compounds, suggesting that these alterations in the structure are responsible for their biological inactivation. The most promising molecules turned out to be **9f**, **12a**, **12b** and **12c**; they exhibited high cytotoxicity to various cancer cells lines. It is important to emphasize that N-1 deprotected pyrazolones **12a** and **12b** were more cytotoxic to cisplatin resistant human laryngeal carcinoma CK2 cells compared to the parental HEp-2 cells. In addition, **12a**, **12b** and **12c** were more cytotoxic to invasive urinary bladder carcinoma T-24 cells than to non-invasive urinary bladder carcinoma RT-112 cells.

It is also interesting to compare the influence of our new compounds on inhibition of tubulin polymerization. The above-mentioned hydrazide **9f**, as well as pyrazolones **12a–12c** and **12f**, are the combretastatin derivatives that possess the best antitubulin potential. Results from the cell cycle analysis of **9f** supported the hypothesis that its antitubulin activity was not altered as compared to CA-4 because **9f** arrested the cells in the G2/M phase of the cell cycle similar to CA-4. In addition, it strongly affected cell shape and microtubule network in a manner comparable to CA-4. Contrary, none of the pyrazolones **11** inhibited tubulin polymerization although some of them were quite cytotoxic (**11a**, **11b**, **11c**, and **11f**), suggesting that the *N*-methoxycarbonyl group on the pyrazolone ring completely blocks the antitubulin potential of those compounds. The molecular modeling results showed that the studied compounds can accommodate into the colchicine binding site at the tubulin heterodimer, and that their specific interactions with the protein are mainly due to differences in the linker. It was also shown that the ADME parameters, for example, lipophilicity, may be important for the biological activity of the ligands.

4. Experimental section

4.1. Chemistry

Starting materials were used as obtained from the commercial sources (Aldrich, Sigma, Fluka). Melting points were determined on a Kofler micro hot stage and are uncorrected. ^{1}H NMR spectra were recorded with a Bruker Avance DPX 300 spectrometer at 29 °C (unless otherwise stated) and 300 MHz, using TMS as an internal standard. ^{13}C NMR spectra were recorded on the same instrument at 75.5 MHz and are referenced against the central line of the solvent signal (DMSO-d_6 septet at δ = 39.5 ppm). IR spectra were obtained with a Bio-Rad FTS 3000MX (KBr pellets for all products). MS spectra were recorded with a VG-Analytical AutoSpec Q instrument. Elemental analyses (C, H, N) were performed with a Perkin–Elmer 2400 Series II CHNS/O Analyzer. TLC was carried out on Fluka silica-gel TLC-cards.

4.1.1. General procedure for the synthesis of acids 7

Triethylamine (5 mL, 35.9 mmol) was added to a stirred mixture of the arylacetic acid (30 mmol), aromatic aldehyde (30 mmol) and acetic anhydride (10 mL, 106 mmol). The reaction mixture was stirred at 100 °C for 6–48 h. The reaction mixture was treated successively with a solution of NaOH and HCl, the resulting water fraction was extracted with CH_2Cl_2 (3 × 100 mL). The organic phase was evaporated to dryness and the raw material was crystallized from a suitable solvent.

4.1.1.1. (*E*)-3-(3-Hydroxy-4-methoxyphenyl)-2-(3,4,5-trimethoxyphenyl)acrylic acid (7a). Yield: 34%; mp 238–239 °C (EtOAc); $mp_{lit.}$ 237–239 °C (EtOH)[33] IR (KBr) 3386, 1678, 1609, 1582, 1509, 1269, 1241, 1128; ^{1}H NMR (DMSO-d_6) δ 3.69 (6H, s), 3.71 (3H, s), 3.73 (3H, s), 6.44 (2H, s), 6.53 (1H, J_1 = 2.1 Hz, d), 6.60 (1H, J_1 = 2.1 Hz, J_2 = 8.4 Hz, dd), 6.80 (1H, J_2 = 8.4 Hz, d), 7.57 (1H, s), 8.92 (1H, s), 12.39 (1H, br s); Calcd for $C_{19}H_{20}O_7$: C, 63.33; H, 5.59. Found: C, 63.34; H, 5.76; ^{13}C NMR (DMSO-d_6) δ 55.5, 56.0, 60.2, 106.9, 111.6, 117.2, 123.1, 127.1, 130.4, 132.2, 137.1, 139.2, 145.9, 148.9, 153.2, 168.6.

4.1.1.2. (*E*)-3-(3-Acetoxy-4-methoxyphenyl)-2-(3,4,5-trimethoxyphenyl)acrylic acid (7a′). Yield: 70%; mp 176.5–178.8 °C (EtOAc); $mp_{lit.}$ not given;[34] IR (KBr) 1665, 1507, 1414, 1289, 1263, 1242, 1206, 1129; ^{1}H NMR (DMSO-d_6) δ 2.17 (3H, s), 3.68 (6H, s), 3.70 (3H, s), 3.74 (3H, s), 6.45 (2H, s), 6.70 (1H, J = 1.2 Hz, d), 7.05 (2H, m), 7.64 (1H, s), 12.52 (1H, br s); MS (ESI) m/z 403.1 (MH^+, 100); Calcd for $C_{21}H_{22}O_8$: C, 62.68; H, 5.51. Found: C, 62.65; H, 5.62.

4.1.1.3. (*E*)-3-(3-Fluoro-4-methoxyphenyl)-2-(3,4,5-trimethoxyphenyl)acrylic acid (7b). Yield: 57%; mp 205–207 °C (EtOAc); $mp_{lit.}$ 203–205 °C (EtOH);[35] IR (KBr) 1672, 1515, 1505, 1414,

1276, 1256, 1242, 1128; ^{1}H NMR (DMSO-d_6) δ 3.69 (6H, s), 3.71 (3H, s), 3.81 (3H, s), 6.46 (2H, s), 6.82 (1H, J_1 = 13.5 Hz, J_2 = 1.8 Hz, dd), 6.98 (1H, J_2 = 1.8 Hz, J_3 = 8.7 Hz, dd), 7.07 (1H, J_3 = 8.7 Hz, t), 7.65 (1H, s), 12.58 (1H, br s).

4.1.1.4. (*E*)-2-(3,4,5-Trimethoxyphenyl)-3-(4-methoxyphenyl)acrylic acid (7c). Yield: 50%; mp 196.3–198.2 °C (EtOAc); $mp_{lit.}$ not given;[36] IR (KBr) 3455, 2942, 1664, 1604, 1273, 1252, 1181, 1127; ^{1}H NMR (DMSO-d_6) δ 3.68 (6H, s), 3.71 (3H, s), 3.72 (3H, s), 6.45 (2H, s), 6.81 and 7.06 (4H, J = 8.7 Hz, AA'XX'), 7.67 (1H, s), 12.45 (1H, br s); Calcd for $C_{19}H_{20}O_6$: C, 66.27; H, 5.85. Found: C, 66.38; H, 6.05.

4.1.1.5. (*E*)-3-(3-Fluorophenyl)-2-(3,4,5-trimethoxyphenyl)acrylic acid (7d). Yield: 60%; mp 215–218 °C (EtOAc); IR (KBr) 2942, 1673, 1584, 1504, 1413, 1294, 1240, 1128; ^{1}H NMR (DMSO-d_6) δ; 3.69 (6H, s), 3.72 (3H, s), 6.49 (2H, s), 6.85 (1H, J_1 = 10.5 Hz, J_2 = 1.8 Hz, dt), 7.01 (1H, J_3 = 7.8 Hz, d), 7.10 (1H, m), 7.30 (1H, m), 7.74 (1H, s), 12.80 (1H, br s); ^{13}C NMR (DMSO-d_6) δ 56.0, 60.2, 106.8, 115.8 (d, J = 21.2 Hz), 116.2 (d, J = 22.5 Hz), 126.5 (d, J = 2.6 Hz), 130.2 (d, J = 8.4 Hz), 131.3, 134.7, 136.9 (d, J = 8.1 Hz), 137.3, 137.4 (d, J = 2.2 Hz), 153.2, 161.7 (d, J = 243.0 Hz), 168.0 MS (ES+) m/z 333.1 (MH^+, 97); HRMS Calcd for $C_{18}H_{18}FO_5$ (MH^+): 333.1138. Found: 333.1132; Calcd for $C_{18}H_{17}FO_5$: C, 65.05; H, 5.16. Found: C, 65.39; H, 5.21.

4.1.1.6. (*E*)-2-(3,4,5-Trimethoxyphenyl)-3-(naphthalen-1-yl)acrylic acid (7e). Yield: 65%; mp 193.7–195.4 °C (EtOAc); IR (KBr) 2939, 1676, 1583, 1505, 1408, 1258, 1237, 1128; ^{1}H NMR (DMSO-d_6) δ 3.46 (6H, s), 3.61 (3H, s), 6.40 (2H, s), 7.15 (1H, m), 7.31 (1H, m), 7.55 (2H, m), 7.82 (1H, m), 7.92 (1H, m), 8.06 (1H, m), 8.36 (1H, s), 12.93 (1H, br s); ^{13}C NMR (DMSO-d_6) δ 55.6, 60.0, 107.6, 124.1, 125.2, 126.1, 126.7, 127.0, 128.45, 128.48, 131.0, 131.1, 132.5, 132.9, 136.1, 137.0, 137.1, 152.3, 168.2; MS (ES+) m/z 365.1 (MH^+, 50); HRMS Calcd for $C_{22}H_{21}O_5$ (MH^+): 365.1389. Found: 365.1387; Calcd for $C_{22}H_{20}O_5$: C, 72.51; H, 5.53. Found: C, 72.76; H, 5.71.

4.1.1.7. (*E*)-2-(3,4,5-Trimethoxyphenyl)-3-(naphthalen-2-yl)acrylic acid (7f). Yield: 53%; mp 257–260 °C (THF/MeOH); IR (KBr) 2938, 1665, 1609, 1582, 1410, 1288, 1236, 1124; ^{1}H NMR (DMSO-d_6) δ 3.65 (6H, s), 3.73 (3H, s), 6.52 (2H, s), 7.03 (1H, m), 7.50 (2H, m), 7.68 (1H, m), 7.80 (3H, m), 7.90 (1H, s), 12.69 (1H, br s); ^{13}C NMR (DMSO-d_6) δ 56.0, 60.2, 107.1, 126.2, 126.5, 127.1, 127.35, 127.41, 128.2, 131.2, 131.7, 132.1, 132.6, 132.8, 133.5, 137.3, 138.8, 153.0, 168.3; MS (ES+) m/z 365.1 (MH^+, 87); HRMS Calcd for $C_{22}H_{21}O_5$ (MH^+): 365.1389. Found: 365.1374; Calcd for $C_{22}H_{20}O_5$: C, 72.51; H, 5.53. Found: C, 71.92; H, 5.63.

4.1.1.8. (*E*)-2-(3,4,5-Trimethoxyphenyl)-3-(3,4-dimethoxyphenyl)-acrylic acid (7g). Yield: 38%; mp 197.9–200.0 °C (EtOAc); IR (KBr) 1664, 1584, 1514, 1414, 1262, 1242, 1165, 1127; ^{1}H NMR (DMSO-d_6) δ 3.37 (3H, s), 3.69 (3H, s), 3.71 (6H, s), 3.73 (3H, s), 6.50 (2H, s), 6.55 (1H, s), 6.88 (2H, s), 7.67 (1H, s), 12.46 (1H, br s); ^{13}C NMR (DMSO-d_6) δ 54.5, 55.4, 56.0, 59.9, 106.8, 111.2, 112.3, 125.5, 126.8, 130.5, 132.5, 136.9, 139.0, 147.9, 149.8, 153.3, 168.4; MS (ESI) m/z 375.2 (MH^+, 100); Calcd for $C_{20}H_{22}O_7$: C, 64.16; H, 5.92. Found: C, 63.89; H, 5.78.

4.1.1.9. (*E*)-3-(3,4,5-Trimethoxyphenyl)-2-(3,4-dimethoxyphenyl)-acrylic acid (7h). Yield: 69%; mp 193.9–196.3 °C (EtOAc); IR (KBr) 1681, 1673, 1509, 1421, 1276, 1251, 1234, 1120; ^{1}H NMR (DMSO-d_6) δ 3.50 (6H, s), 3.63 (3H, s), 3.70 (3H, s), 3.77 (3H, s), 6.47 (2H, s), 6.73 (1H, J_1 = 8.4 Hz, J_2 = 1.8 Hz, dd), 6.81 (1H, J_2 = 1.8 Hz, d), 7.67 (1H, J_1 = 8.4 Hz, d), 7.69 (1H, s), 12.54 (1H, br s); ^{13}C NMR (DMSO-d_6) δ 55.3, 55.7, 55.7, 60.0, 108.1, 112.3, 113.5, 121.9, 129.0, 129.8, 132.2, 138.3, 138.9, 148.5, 149.1, 152.3, 168.5; MS (ESI) m/z 375.1 (MH^+, 44); Calcd for $C_{20}H_{22}O_7$: C, 64.16; H, 5.92. Found: C, 64.07; H, 5.90.

4.1.1.10. (*E*)-3-(2,4,5-Trimethoxyphenyl)-2-(3,4-dimethoxyphenyl)-acrylic acid (7i). Yield: 63%; mp 205–207 °C (EtOAc); mp_{lit} not given;[37] IR (KBr) 1665, 1592, 1511, 1460, 1274, 1253, 1220, 1028; ^{1}H NMR (DMSO-d_6) δ 3.16 (3H, s), 3.69 (3H, s), 3.76 (3H, s), 3.80 (3H, s), 3.87 (3H, s), 6.26 (1H, s), 6.65 (1H, s), 6.71 (1H, J_1 = 1.5 Hz, J_2 = 8.4 Hz, dd), 6.80 (1H, J_1 = 1.5 Hz, d), 6.97 (1H, J_2 = 8.4 Hz, d), 8.05 (1H, s), 12.36 (1H, br s); ^{13}C NMR (DMSO-d_6) δ 54.9, 55.6, 55.7, 55.7, 56.3, 97.3, 112.3, 112.8, 113.8, 114.0, 122.2, 129.6, 129.7, 133.0, 141.7, 148.3, 149.1, 151.0, 153.6, 168.9; MS (ESI) m/z 375.1 (MH^+, 70); HRMS Calcd for $C_{20}H_{23}O_7$ (MH^+): 375.1444. Found: 375.1439; Calcd for $C_{20}H_{22}O_7$: C, 64.16; H, 5.92. Found: C, 64.15; H, 6.02.

4.1.2. General procedure for the preparation of hydrazides 9

Oxalyl chloride (2.54 g, 20 mmol) was slowly added to a stirred mixture of the appropriate acid **7** (10 mmol) and *N*,*N*-dimethylformamide (2–3 drops) in dry CH_2Cl_2 (20 mL) at 0 °C under argon. The reaction mixture was stirred at rt for the additional 2–5 h and evaporated to dryness to give the corresponding acid chloride in quantitative yield. Then, a solution of the chloride (10 mmol) in dry CH_2Cl_2 (20 mL) was slowly added to a stirred solution of methyl carbazate (902 mg, 10 mmol) and pyridine (0.845 mL, 10.4 mmol) in dry CH_2Cl_2 (20 mL) at 0 °C. The reaction mixture was then stirred at rt for 15−23 h, water was added (20 mL). The organic phase was separated and evaporated to dryness to give the methyl prop-2-enoylhydrazinecarboxylate **9** in excellent yield.

4.1.2.1. Methyl 2-[(2*E*)-(2-(3,4,5-trimethoxyphenyl)-3-(3-acetoxy-4-methoxyphenyl))prop-2-enoyl]hydrazinecarboxylate (9a). Yield: 100%; mp 152.8–154.5 °C (EtOAc/heptane); IR (KBr) 3340, 1741, 1668, 1587, 1509, 1242, 1202, 1123; ^{1}H NMR (DMSO-d_6) δ 2.18 (3H, s), 3.61 (3H, s), 3.69 (6H, s), 3.72 (3H, s), 3.75 (3H, s), 6.48 (2H, s), 6.70 (1H, J_1 = 1.5 Hz, d), 7.05 (2H, m), 7.30 (1H, s), 9.10 (1H, br s), 9.36 (1H, br s); ^{13}C NMR (DMSO-d_6) δ 20.2, 51.9, 55.8, 60.1, 106.7, 112.5, 124.0, 127.3, 129.1, 130.5, 133.3, 133.4, 137.7, 138.8, 151.2, 153.4, 156.7, 167.4, 168.3; MS (ES+) m/z (%) 497.2 (MNa^+, 47); HRMS Calcd for $C_{23}H_{26}N_2O_9Na$ (MNa^+): 497.1536. Found: 497.1527; Calcd for $C_{23}H_{26}N_2O_9$: C, 58.22; H, 5.52; N, 5.90. Found: C, 58.14; H, 5.78; N, 5.61.

4.1.2.2. Methyl 2-[(2*E*)-(2-(3,4,5-trimethoxyphenyl)-3-(3-fluoro-4-methoxyphenyl))prop-2-enoyl]hydrazinecarboxylate (9b). Yield: 100%; mp 151.8–154.3 °C (EtOAc); IR (KBr) 3331, 1748, 1666, 1512, 1451, 1271, 1236, 1126; ^{1}H NMR (DMSO-d_6) δ 3.62 (3H, s), 3.70 (6H, s), 3.73 (3H, s), 3.81 (3H, s), 6.49 (2H, s), 6.81 (1H, m), 6.98 (1H, m), 7.07 (1H, m), 7.31 (1H, s), 9.11 (1H, br s), 9.35 (1H, br s); ^{13}C NMR (DMSO-d_6) δ 51.9, 55.9, 56.0, 60.1, 106.7, 113.4, 116.5 (d, J = 19.0 Hz), 127.2 (d, J = 2.0 Hz), 127.6 (d, J = 6.8 Hz), 130.4, 133.2, 133.7, 137.6, 147.4 (d, J = 10.7 Hz), 150.7 (d, J = 243.3 Hz), 153.4, 156.6, 167.2; MS (ES+) m/z (%) 457.1 (MNa^+, 100); HRMS Calcd for $C_{21}H_{23}FN_2O_7Na$ (MNa^+): 457.1387. Found: 457.1388; Calcd for $C_{21}H_{23}FN_2O_7$: C, 58.06; H, 5.34; N, 6.45. Found: C, 57.94; H, 5.40; N, 6.50.

4.1.2.3. Methyl 2-[(2*E*)-(2-(3,4,5-trimethoxyphenyl)-3-(4-methoxyphenyl))prop-2-enoyl]hydrazinecarboxylate (9c). Yield: 100%; mp 118.9–121.3 °C (EtOAc); IR (KBr) 3313, 1743, 1664, 1602, 1583, 1512, 1462, 1244, 1126; ^{1}H NMR (DMSO-d_6) δ 3.61 (3H, s), 3.68 (6H, s), 3.72 (3H, s), 3.73 (3H, s), 6.48 (2H, s), 6.81 and 7.06 (4H, J = 8.7 Hz, AA'XX'), 7.32 (1H, s), 9.09 (1H, br s), 9.30 (1H, br s); ^{13}C NMR (DMSO-d_6) δ 51.9, 55.1, 55.8, 60.1, 106.8, 113.8, 127.0, 130.9, 131.5, 132.4, 134.2, 137.4, 153.3,

156.7, 159.5, 167.6; MS (ES+) *m*/*z* (%) 439.1 (MNa^+, 100); HRMS Calcd for $C_{21}H_{24}N_2O_7Na$ (MNa^+): 439.1481. Found: 439.1481.

4.1.2.4. Methyl 2-[(2*E*)-(2-(3,4,5-trimethoxyphenyl)-3-(3-fluorophenyl))prop-2-enoyl]hydrazinecarboxylate (9d). Yield: 98%; mp 142.3–143.8 °C (EtOAc); IR (KBr) 3333, 3240, 1743, 1668, 1585, 1506, 1236, 1125; ^{1}H NMR (DMSO-d_6) δ 3.63 (3H, s), 3.67 (6H, s), 3.72 (3H, s), 6.49 (2H, s), 6.86 (1H, m), 7.00 (1H, m), 7.09 (1H, m), 7.31 (2H, m), 9.17 (1H, br s), 9.56 (1H, br s); ^{13}C NMR (DMSO-d_6) δ 51.9, 55.9, 60.1, 106.8, 115.2 (d, J = 21.1 Hz), 115.8 (d, J = 22.3 Hz), 126.0 (d, J = 2.0 Hz), 130.0, 130.2 (d, J = 8.5 Hz), 132.7, 136.4, 137.3 (d, J = 8.0 Hz), 137.7, 153.2, 156.7, 161.8 (d, J = 243.0 Hz), 167.4; MS (ES+) *m*/*z* (%) 405.1 (MH^+, 16); HRMS Calcd for $C_{20}H_{22}FN_2O_6$ (MH^+): 405.1462. Found: 405.1471; Calcd for $C_{20}H_{21}FN_2O_6$: C, 59.40; H, 5.23; N, 6.93. Found: C, 59.25; H, 5.24; N, 6.79.

4.1.2.5. Methyl 2-[(2*E*)-(2-(3,4,5-trimethoxyphenyl)-3-(naphthalen-1-yl))prop-2-enoyl]hydrazinecarboxylate (9e). Yield: 99%; mp 181.4–182.9 °C (EtOAc); IR (KBr) 3336, 3232, 1740, 1661, 1585, 1501, 1238, 1121; ^{1}H NMR (DMSO-d_6) δ 3.39 (6H, s), 3.59 (3H, s), 3.67 (3H, s), 6.39 (2H, s), 7.19 (1H, m), 7.37 (1H, m), 7.55 (2H, m), 7.69 (1H, s), 7.84, (1H, m), 7.93 (1H, m), 8.09 (1H, m), 9.28 (1H, br s), 10.02 (1H, br s); ^{13}C NMR (DMSO-d_6) δ 52.0, 55.4, 59.9, 107.1, 124.4, 125.3, 126.1, 126.5, 126.7, 128.0, 128.4, 130.1, 131.1, 131.2, 133.0, 137.1, 138.0, 152.3, 156.8, 168.3; MS (ES+) *m*/*z* (%) 435.2 ([[M−2]+H]$^+$, 10); HRMS Calcd for $C_{24}H_{23}N_2O_6$ ([[M−2]+H]$^+$): 435.1556. Found: 435.1555; Calcd for $C_{24}H_{24}N_2O_6$: C, 66.04; H, 5.54; N, 6.42. Found: C, 66.11; H, 5.57; N, 6.41.

4.1.2.6. Methyl 2-[(2*E*)-(2-(3,4,5-trimethoxyphenyl)-3-(naphthalen-2-yl))prop-2-enoyl]hydrazinecarboxylate (9f). Yield: 100%; mp 189.8–192.9 °C (EtOAc); IR (KBr) 3316, 3244, 1742, 1661, 1612, 1503, 1240, 1121; ^{1}H NMR (DMSO-d_6) δ 3.63 (6H, s), 3.66 (3H, s), 3.75 (3H, s), 6.56 (2H, s), 7.10 (1H, m), 7.50 (3H, m), 7.70 (1H, m), 7.80 (3H, m), 9.21 (1H, br s), 9.60 (1H, br s); ^{13}C NMR (DMSO-d_6) δ 51.9, 55.8, 60.1, 107.1, 126.2, 126.5, 126.8, 127.3, 127.4, 128.1, 130.3, 130.5, 132.5, 132.6, 132.7, 134.1, 135.3, 137.7, 153.2, 156.7, 167.7; MS (ES+) *m*/*z* (%) 459.2 (MNa^+, 8); HRMS Calcd for $C_{24}H_{24}N_2O_6Na$ (MNa^+): 459.1532. Found: 459.1532; Calcd for $C_{24}H_{24}N_2O_6$: C, 66.04; H, 5.54; N, 6.42. Found: C, 66.08; H, 5.41; N, 6.14.

4.1.2.7. Methyl 2-[(2*E*)-(2-(3,4,5-trimethoxyphenyl)-3-(3,4-dimethoxyphenyl))prop-2-enoyl]hydrazinecarboxylate (9g). Yield: 99%; mp 106.3–109.5 °C (EtOAc/hexane); IR (KBr) 3326, 1738, 1663, 1514, 1272, 1247, 1236, 1125; ^{1}H NMR (DMSO-d_6) δ 3.40 (3H, s), 3.61 (3H, s), 3.70 (3H, s), 3.72 (6H, s), 3.73 (3H, s), 6.51 (2H, s), 6.54 (1H, J_1 = 1.5 Hz, d), 6.86 (2H, m), 7.37 (1H, s), 9.08 (1H, br s), 9.24 (1H, br s); ^{13}C NMR (DMSO-d_6) δ 51.9, 54.6, 55.4, 56.0, 59.4, 106.9, 111.3, 112.1, 124.5, 127.1, 131.1, 132.2, 134.9, 137.4, 147.9, 149.4, 153.5, 156.7, 167.2; MS (ES+) *m*/*z* (%) 469.2 (MNa^+, 100); HRMS Calcd for $C_{22}H_{26}N_2O_8Na$ (MNa^+): 469.1587. Found: 469.1589; Calcd for $C_{22}H_{26}N_2O_8$: C, 59.19; H, 5.87; N, 6.27. Found: C, 59.11; H, 5.91; N, 6.24.

4.1.2.8. Methyl 2-[(2*E*)-(2-(3,4-dimethoxyphenyl)-3-(3,4,5-trimethoxyphenyl))prop-2-enoyl]hydrazinecarboxylate (9h). Yield: 99%; mp 187.1–188.6 °C (EtOAc); IR (KBr) 3351, 1746, 1667, 1580, 1509, 1257, 1237, 1126; ^{1}H NMR (DMSO-d_6) δ 3.51 (6H, s), 3.60 (3H, s), 3.62 (3H, s), 3.69 (3H, s), 3.77 (3H, s), 6.41 (2H, s), 6.75 (2H, m), 7.03 (1H, J = 8.4 Hz, d), 7.31 (1H, s), 9.09 (1H, br s), 9.30 (1H, br s); ^{13}C NMR (DMSO-d_6) δ; 51.9, 55.4, 55.6, 55.7, 60.0, 107.6, 112.5, 113.3, 122.1, 127.7, 130.1, 133.9, 134.5, 137.8, 148.8, 149.2, 152.3, 156.7, 167.5; MS (ES+) *m*/*z* (%) 469.2 (MNa^+, 100); HRMS Calcd for $C_{22}H_{26}N_2O_8Na$ (MNa^+): 469.1587. Found: 469.1577; Calcd for $C_{22}H_{26}N_2O_8$: C, 59.19; H, 5.87; N, 6.27. Found: C, 59.24; H, 5.91; N, 6.04.

4.1.2.9. Methyl 2-[(2*E*)-(2-(3,4-dimethoxyphenyl)-3-(2,4,5-trimethoxyphenyl))prop-2-enoyl]hydrazinecarboxylate (9i). Yield: 99%; mp 174.0–176.7 °C (EtOAc/heptane); IR (KBr) 3370, 1653, 1511, 1470, 1290, 1255, 1219, 1023; ^{1}H NMR (DMSO-d_6) δ 3.17 (3H, s), 3.60 (3H, s), 3.66 (3H, s), 3.75 (3H, s), 3.78 (3H, s), 3.83 (3H, s), 6.24 (1H, s), 6.65 (1H, s), 6.69 (1H, J_1 = 1.8 Hz, J_2 = 8.1 Hz, dd), 6.75 (1H, J_1 = 1.8 Hz, d), 6.98 (1H, J_2 = 8.1 Hz, d), 7.53 (1H, s), 9.03 (1H, br s), 9.22 (1H, br s); ^{13}C NMR (DMSO-d_6) δ 51.9, 55.1, 55.6, 55.7, 56.3, 97.4, 112.4, 112.9, 113.5, 114.4, 122.3, 128.4, 128.8, 131.9, 141.7, 148.7, 149.1, 150.4, 153.2, 156.7, 168.1; MS (ESI) *m*/*z* 447.2 (MH^+, 15); Calcd for $C_{22}H_{26}N_2O_8$: C, 59.19; H, 5.87; N, 6.27. Found: C, 59.46; H, 6.07; N, 6.37.

4.1.3. Oxidation of hydrazides 9 to diazenes 10 and their cyclization into 11

NBS (1.584 g, 8.8 mmol) was slowly added to a stirred solution of the hydrazide **9** (8 mmol) and pyridine (1.28 g, 16 mmol) in CH_2Cl_2 (105 mL) at room temperature. The reaction mixture was then stirred at the same temperature for 5–10 min, treated successively with a 12% solution of HCl (30 mL), 5% solution of $Na_2S_2O_3 \times 5H_2O$ (30 mL), saturated aqueous $NaHCO_3$ (30 mL) and H_2O (30 mL) and dried over anhydrous Na_2SO_4. Organic phase containing the diazene was refluxed for 1−4 h. The reaction mixture was then evaporated to dryness to give the products **11** in good to excellent yield.

4.1.3.1. Methyl 5-(3-acetoxy-4-methoxyphenyl)-2,3-dihydro-4-(3,4,5-trimethoxyphenyl)-3-oxopyrazole-1-carboxylate (11a). Yield: 93%; mp 205–208 °C (EtOAc); IR (KBr) 1758, 1541, 1437, 1352, 1270, 1252, 1198, 1123; ^{1}H NMR (DMSO-d_6) δ 2.24 (3H, s), 3.54 (6H, s), 3.61 (3H, s), 3.74 (3H, s), 3.80 (3H, s), 6.50 (2H, s), 7.14 (2H, m), 7.19 (1H, m), 11.55 (1H, br s); ^{13}C NMR (DMSO-d_6) δ 20.3, 53.9, 55.4, 55.9, 59.9, 105.9, 112.1, 112.4, 123.4, 124.7, 125.4, 128.5, 136.3, 139.0, 141.4, 149.7, 151.2, 152.3, 160.5, 168.3; MS (ESI) *m*/*z* 473.1 (MH^+, 100); Calcd for $C_{23}H_{24}N_2O_9$: C, 58.47; H, 5.12; N, 5.93. Found: C, 58.11; H, 5.34; N, 5.79.

4.1.3.2. Methyl 2,3-dihydro-4-(3,4,5-trimethoxyphenyl)-5-(3-fluoro-4-methoxyphenyl)-3-oxopyrazole-1-carboxylate (11b). Yield: 87%; mp 201–203 °C (EtOAc); IR (KBr) 2836, 1755, 1580, 1542, 1435, 1352, 1250, 1121; ^{1}H NMR (DMSO-d_6) δ 3.56 (6H, s), 3.63 (3H, s), 3.76 (3H, s), 3.87 (3H, s), 6.52 (2H, s), 7.10 (1H, m), 7.18 (1H, m), 7.34 (1H, m), 11.56 (1H, br s); ^{13}C NMR (DMSO-d_6) δ 53.9, 55.5, 56.1, 60.0, 106.2, 112.4, 113.3, 117.8 (d, J = 19.1 Hz), 123.6 (d, J = 7.6 Hz), 125.4, 126.7 (d, J = 2.9 Hz), 136.5, 141.2, 147.5 (d, J = 10.4 Hz), 149.7, 151.0 (d, J = 243.9 Hz), 152.6, 160.6; MS (ES+) *m*/*z* (%) 433.1 (MH^+, 20); HRMS Calcd for $C_{21}H_{22}FN_2O_7$ (MH^+): 433.1411. Found: 433.1410; Calcd for $C_{21}H_{21}FN_2O_7$: C, 58.33; H, 4.90; N, 6.48. Found: C, 58.41; H, 4.66; N, 6.44.

4.1.3.3. Methyl 2,3-dihydro-4-(3,4,5-trimethoxyphenyl)-5-(4-methoxyphenyl)-3-oxopyrazole-1-carboxylate (11c). Yield: 86%; mp 206–211 °C (EtOAc); IR (KBr) 3464, 1763, 1613, 1536, 1412, 1346, 1249, 1126; ^{1}H NMR (DMSO-d_6) δ 3.52 (6H, s), 3.61 (3H, s), 3.73 (3H, s), 3.78 (3H, s), 6.48 (2H, s), 6.97 and 7.26 (4H, J = 8.7 Hz, AA'XX'), 11.51 (1H, br s); ^{13}C NMR (DMSO-d_6) δ 53.8, 55.2, 55.4, 59.9, 106.0, 111.9, 113.5, 123.1, 125.6, 131.3, 136.2, 142.6, 149.7, 152.2, 159.4, 160.5; MS (ESI) *m*/*z* 415.1 (MH^+, 100); Calcd for $C_{21}H_{22}N_2O_7$: C, 60.86; H, 5.35; N, 6.76. Found: C, 60.97; H, 5.47; N, 6.68.

4.1.3.4. Methyl 2,3-dihydro-4-(3,4,5-trimethoxyphenyl)-5-(3-fluorophenyl)-3-oxopyrazole-1-carboxylate (11d). Yield: 97%; mp 203–205 °C (EtOAc); IR (KBr) 1761, 1587, 1511, 1439, 1415, 1339, 1244, 1127; ^{1}H NMR (DMSO-d_6) δ 3.54 (6H, s), 3.62 (3H, s), 3.76 (3H, s), 6.51 (2H, s), 7.26 (3H, m), 7.46 (1H, m), 11.64 (1H, br s); ^{13}C NMR (DMSO-d_6) δ 54.0, 55.4, 60.0, 106.1, 112.5, 115.5 (d, J = 20.9 Hz), 117.1 (d, J = 22.4 Hz), 125.1, 126.3 (d, J = 2.0 Hz), 130.1 (d, J = 8.5 Hz), 133.6 (d, J = 8.8 Hz), 136.5, 141.0 (d, J = 1.8 Hz), 149.7, 152.4, 160.6, 161.8 (d, J = 243.9 Hz); MS (ES+) m/z (%) 403.1 (MH$^+$, 67); Calcd for $C_{20}H_{19}FN_2O_6$: C, 59.70; H, 4.76; N, 6.96. Found: C, 59.66; H, 4.92; N, 6.90.

4.1.3.5. Methyl 2,3-dihydro-4-(3,4,5-trimethoxyphenyl)-5-(naphthalen-1-yl)-3-oxopyrazole-1-carboxylate (11e). Yield: 100%; mp 223–225 °C (EtOAc); IR (KBr) 2953, 1749, 1608, 1504, 1440, 1354, 1256, 1130; ^{1}H NMR (DMSO-d_6) δ 3.25 (6H, s), 3.52 (3H, s), 3.62 (3H, s), 6.46 (2H, s), 7.52 (5H, m), 8.01 (2H, m), 11.81 (1H, br s); ^{13}C NMR (DMSO-d_6) δ 53.9, 55.0, 59.9, 105.2, 112.9, 124.7, 125.4, 125.5, 126.2, 127.1, 127.9, 128.3, 129.0, 129.4, 132.1, 132.9, 136.3, 140.5, 149.4, 152.2, 160.9; MS (ES+) m/z 435.2 (MH$^+$, 100); Calcd for $C_{24}H_{22}N_2O_6$: C, 66.35; H, 5.10; N, 6.45. Found: C, 66.14; H, 5.27; N, 6.36.

4.1.3.6. Methyl 2,3-dihydro-4-(3,4,5-trimethoxyphenyl)-5-(naphthalen-2-yl)-3-oxopyrazole-1-carboxylate (11f). Yield: 89%; mp 212–215 °C (EtOAc); IR (KBr) 2943, 1750, 1593, 1508, 1436, 1352, 1249, 1123; ^{1}H NMR (DMSO-d_6) δ 3.36 (6H, s), 3.55 (3H, s), 3.72 (3H, s), 6.51 (2H, s), 7.54 (3H, m), 7.93 (4H, m), 11.66 (1H, br s); ^{13}C NMR (DMSO-d_6) δ 53.9, 55.2, 59.9, 106.1, 112.5, 125.4, 126.4, 126.8, 127.4, 127.5, 127.7, 127.9, 128.8, 128.9, 132.4, 132.6, 136.3, 142.5, 149.8, 152.2, 160.7; MS (ES+) m/z 435.2 (MH$^+$, 45); Calcd for $C_{24}H_{22}N_2O_6$: C, 66.35; H, 5.10; N, 6.45. Found: C, 66.34; H, 5.14; N, 6.43.

4.1.3.7. Methyl 2,3-dihydro-4-(3,4,5-trimethoxyphenyl)-5-(3,4-dimethoxyphenyl)-3-oxopyrazole-1-carboxylate (11g). Yield: 95%; mp 205–208 °C (EtOAc); IR (KBr) 1764, 1584, 1438, 1414, 1351, 1248, 1139, 1126; ^{1}H NMR (DMSO-d_6) δ 3.53 (6H, s), 3.61 (3H, s), 3.68 (3H, s), 3.74 (3H, s), 3.78 (3H, s), 6.53 (2H, s), 6.83 (1H, J_1 = 8.4 Hz, J_2 = 1.8 Hz, dd), 6.97 (1H, J_1 = 8.4 Hz, d), 7.00 (1H, J_2 = 1.8 Hz, d), 11.50 (1H, br s); ^{13}C NMR (DMSO-d_6) δ 53.8, 55.4, 55.5, 55.8, 59.9, 106.0, 111.4, 111.9, 114.0, 122.5, 123.4, 125.7, 136.3, 142.6, 148.4, 149.2, 149.7, 152.2, 160.5; MS (ESI) m/z 445.1 (MH$^+$, 100); HRMS Calcd for $C_{22}H_{25}N_2O_8$ [M+H]$^+$: 445.1611 Found: 445.1622; Calcd for $C_{22}H_{24}N_2O_8$: C, 59.45; H, 5.44; N, 6.30. Found: C, 59.58; H, 5.51; N, 6.24.

4.1.3.8. Methyl 2,3-dihydro-5-(3,4,5-trimethoxyphenyl)-4-(3,4-dimethoxyphenyl)-3-oxopyrazole-1-carboxylate (11h). Yield: 92%; mp 210–215 °C (EtOAc); IR (KBr) 1757, 1584, 1545, 1438, 1350, 1251, 1240, 1131; ^{1}H NMR (DMSO-d_6) δ 3.45 (3H, s), 3.68 (6H, s), 3.69 (3H, s), 3.70 (3H, s), 3.75 (3H, s), 6.67 (1H, s), 6.70 (1H, J_1 = 1.8 Hz, d) 6.86 (1H, J_2 = 8.4 Hz, d), 6.97 (1H, J_1 = 8.4 Hz, J_2 = 1.8 Hz, dd), 11.46 (1H, s); ^{13}C NMR (DMSO-d_6) δ 53.8, 54.8, 55.3, 56.1, 60.0, 107.7, 111.4, 111.9, 112.0, 121.0, 122.5, 126.7, 137.7, 141.9, 147.6, 147.8, 149.6, 152.6, 160.6; MS (ESI) m/z 445.1 (MH$^+$, 100); Calcd for $C_{22}H_{24}N_2O_8$: C, 59.45; H, 5.44; N, 6.30. Found: C, 59.57; H, 5.30; N, 6.34.

4.1.3.9. Methyl 2,3-dihydro-5-(2,4,5-trimethoxyphenyl)-4-(3,4-dimethoxyphenyl)-3-oxopyrazole-1-carboxylate (11i). Yield: 88%; mp 206–209 °C (EtOAc); IR (KBr) 1759, 1543, 1442, 1348, 1264, 1251, 1212, 1028; ^{1}H NMR (DMSO-d_6) δ 3.50 (3H, s), 3.58 (3H, s), 3.68 (3H, s), 3.69 (3H, s), 3.74 (3H, s), 3.85 (3H, s), 6.75 (1H, s), 6.77 (1H, J_1 = 1.8 Hz, d), 6.78 (1H, s), 6.84 (1H, J_2 = 8.4 Hz, d), 6.93 (1H, J_1 = 1.8 Hz, J_2 = 8.4 Hz, dd), 11.38 (1H, br s); ^{13}C NMR (DMSO-d_6) δ 53.7, 55.0, 55.4, 55.8, 56.3, 56.5, 98.1, 111.2, 111.5, 111.8, 112.0, 115.2, 120.8, 123.0, 139.0, 142.5, 147.7, 148.0, 149.7, 150.5, 152.3, 160.8; MS (ESI) m/z 445.1 (MH$^+$, 100); Calcd for $C_{22}H_{24}N_2O_8$: C, 59.45; H, 5.44; N, 6.30. Found: C, 59.64; H, 5.21; N, 6.35.

4.1.4. Conversion of 11 into 12

A methanolic solution of NaOH (2 N, 2.4 mL) was added to a stirred mixture of **11** (2 mmol) in CH_2Cl_2/MeOH (9:1; 8 mL) at rt. Stirring was continued at the same temperature for additional 1–5 h and the reaction mixture was evaporated to dryness. The residue was treated with water (5 mL), made acidic with HCl (1:2, v/v) and extracted with EtOAc (3 × 30 mL). The combined EtOAc extracts were dried over anhydrous sodium sulfate and evaporated to dryness to give the corresponding combretastatins **12**.

4.1.4.1. 1,2-Dihydro-5-(3-hydroxy-4-methoxyphenyl)-4-(3,4,5-trimethoxyphenyl)pyrazol-3-one (12a). Yield: 100%; mp 253–256 °C (EtOAc); IR (KBr) 3232, 1582, 1519, 1501, 1439, 1243, 1218, 1101; ^{1}H NMR (DMSO-d_6) δ 3.60 (6H, s), 3.65 (3H, s), 3.77 (3H, s), 6.59 (2H, s), 6.82 (2H, m), 6.95 (1H, m), 9.08 (1H, br s), 10.06 (1H, br s), 11.65 (1H, br s); ^{13}C NMR (DMSO-d_6) δ 55.6, 55.6, 60.0, 102.0, 106.1, 112.2, 115.2, 119.0, 123.4, 128.4, 135.5, 139.8, 146.3, 147.7, 152.4, 158.9; MS (ESI) m/z 373.1 (MH$^+$, 100); Calcd for $C_{19}H_{20}N_2O_6$: C, 61.28; H, 5.41; N, 7.52. Found: C, 61.03; H, 5.51; N, 7.30.

4.1.4.2. 5-(3-Fluoro-4-methoxyphenyl)-1,2-dihydro-4-(3,4,5-trimethoxyphenyl)pyrazol-3-one (12b). Yield: 89%; mp 241–243 °C (EtOAc); IR (KBr) 3266, 1583, 1531, 1498, 1416, 1269, 1240, 1119; ^{1}H NMR (DMSO-d_6) δ 3.65 (6H, s), 3.68 (3H, s), 3.86 (3H, s), 6.60 (2H, s), 7.23 (3H, m), 11.04 (1H, br s); ^{13}C NMR (DMSO-d_6) δ 55.7, 56.1, 60.1, 102.7, 106.5, 113.9 (d, J = 1.8 Hz), 115.0 (d, J = 19.2 Hz), 123.5 (d, J = 7.2 Hz), 124.2 (d, J = 3.2 Hz), 128.1, 135.9, 138.5, 147.0 (d, J = 10.5 Hz), 151.2 (d, J = 243.8 Hz), 152.6, 158.8; MS (ES+) m/z 375.1 (MH$^+$, 29); HRMS Calcd for $C_{19}H_{20}FN_2O_5$ (MH$^+$): 375.1356. Found: 375.1356; Calcd for $C_{19}H_{19}FN_2O_5$: C, 60.96; H, 5.12; N, 7.48. Found: C, 60.94; H, 5.11; N, 7.30.

4.1.4.3. 1,2-Dihydro-4-(3,4,5-trimethoxyphenyl)-5-(4-methoxyphenyl)pyrazol-3-one (12c). Yield: 60%; mp 245–249 °C (EtOAc); IR (KBr) 3265, 1616, 1590, 1528, 1512, 1251, 1123, 841; ^{1}H NMR (DMSO-d_6) δ 3.60 (6H, s), 3.65 (3H, s), 3.76 (3H, s), 6.56 (2H, s), 6.97 and 7.33 (4H, J = 8.7 Hz, AA'XX'), 10.10 (1H, br s), 11.74 (1H, br s); ^{13}C NMR (DMSO-d_6) δ 55.2, 55.5, 60.0, 102.1, 106.1, 113.9, 123.0, 128.4, 129.1, 135.5, 139.5, 152.4, 158.9, 159.1; MS (ESI) m/z 357.1 (MH$^+$, 100); Calcd for $C_{19}H_{20}N_2O_5$: C, 64.04; H, 5.66; N, 7.86. Found: C, 63.82; H, 5.79; N, 7.72.

4.1.4.4. 1,2-Dihydro-5-(3-fluorophenyl)-4-(3,4,5-trimethoxyphenyl)pyrazol-3-one (12d). Yield: 100%; mp 262–265 °C (EtOAc); IR (KBr) 3352, 1585, 1518, 1468, 1413, 1236, 1128, 879; ^{1}H NMR (DMSO-d_6) δ 3.63 (6H, s), 3.67 (3H, s), 6.57 (2H, s), 7.20 (3H, m), 7.44 (1H, m), 10.38 (1H, br s), 11.88 (1H, br s); ^{13}C NMR (DMSO-d_6) δ 55.6, 60.0, 103.2, 106.5, 114.2 (d, J = 22.6 Hz), 114.8 (d, J = 20.7 Hz), 123.8, 127.8, 130.5 (d, J = 6.2 Hz), 133.0, 135.9, 138.5, 152.6, 158.7, 162.0 (d, J = 243.4 Hz); MS (ES+) m/z (%) 345.1 (MH$^+$, 100); HRMS Calcd for $C_{18}H_{18}FN_2O_4$ (MH$^+$): 345.1251. Found: 345.1252; Calcd for $C_{18}H_{17}FN_2O_4$: C, 62.79; H, 4.98; N, 8.14. Found: C, 62.66; H, 5.01; N, 7.93.

4.1.4.5. 1,2-Dihydro-4-(3,4,5-trimethoxyphenyl)-5-(naphthalen-1-yl)pyrazol-3-one (12e). Yield: 92%; mp 290–294 °C (EtOAc); IR (KBr) 3264, 1604, 1588, 1531, 1518, 1416, 1246, 1126; ^{1}H NMR (DMSO-d_6) δ 3.24 (6H, s), 3.51 (3H, s), 6.49 (2H, s), 7.53 (5H, m), 8.03 (2H, m), 10.65 (1H, br s), 11.81 (1H, br s); ^{13}C NMR (DMSO-

d_6) δ 55.0, 59.9, 103.6. 104.1, 125.4, 125.5, 126.2, 126.7, 128.2, 128.3, 128.5, 129.0, 129.4, 131.6, 133.1, 134.8, 138.3, 152.2, 158.5; MS (ES+) m/z 377.1 (MH^+, 100); HRMS Calcd for $C_{22}H_{21}N_2O_4$ (MH^+): 377.1501. Found: 377.1495.

4.1.4.6. 1,2-Dihydro-4-(3,4,5-trimethoxyphenyl)-5-(naphthalen-2-yl)pyrazol-3-one (12f). Yield: 78%; mp 271–273 °C (MeOH/EtOAc); IR (KBr) 3262, 2934, 1589, 1520, 1414, 1334, 1248, 1124; ^{1}H NMR (DMSO-d_6) δ 3.54 (6H, s), 3.67 (3H, s), 6.65 (2H, s), 7.51 (3H, m), 7.90 (3H, m), 8.06 (1H, m), 11.23 (2H, br s); ^{13}C NMR (DMSO-d_6) δ 55.6, 60.1, 103.0, 106.3, 125.9, 126.5, 126.6, 127.6, 127.8, 127.9, 128.2, 128.3, 132.4, 132.8, 135.8, 139.8, 152.5, 159.0; MS (ES+) m/z 377.1 (MH^+, 58); Calcd for $C_{22}H_{20}N_2O_4$: C, 70.20; H, 5.36; N, 7.44. Found: C, 70.02; H, 5.49; N, 7.42.

4.1.4.7. 1,2-Dihydro-4-(3,4,5-trimethoxyphenyl)-5-(3,4-dimethoxyphenyl)pyrazol-3-one (12g). Yield: 100%; mp 249–250 °C (EtOAc); IR (KBr) 3295, 2938, 1589, 1524, 1460, 1412, 1243, 1121; ^{1}H NMR (DMSO-d_6) δ 3.64 (6H, s), 3.66 (3H, s), 3.67 (3H, s), 3.77 (3H, s), 6.62 (2H, s), 7.00 (3H, m), 11.01 (2H, br s); ^{13}C NMR (DMSO-d_6) δ 55.3, 55.5, 55.7, 60.0, 102.3, 106.5, 111.4, 111.8, 120.1, 123.1, 128.5, 135.8, 139.6, 148.5, 148.8, 152.5, 159.0; MS (ES+) m/z 387.2 (MH^+, 100); HRMS Calcd for $C_{20}H_{23}N_2O_6$ (MH^+): 387.1556. Found: 387.1565; Calcd for $C_{20}H_{22}N_2O_6$: C, 62.17; H, 5.74; N, 7.25. Found: C, 62.36; H, 5.56; N, 7.27.

4.1.4.8. 1,2-Dihydro-5-(3,4,5-trimethoxyphenyl)-4-(3,4-dimethoxyphenyl)pyrazol-3-one (12h). Yield: 100%; mp 239–242 °C (EtOAc); IR (KBr) 3315, 1585, 1576, 1519, 1417, 1248, 1216, 1128; ^{1}H NMR (DMSO-d_6) δ 3.65 (9H, br s), 3.68 (3H, s), 3.75 (3H, s), 6.74 (2H, s), 6.91 (3H, m), 11.01 (2H, br s); ^{13}C NMR (DMSO-d_6) δ 55.4, 55.6, 55.7, 60.1, 102.7, 104.8, 111.9, 113.5, 121.8, 125.4, 126.0, 137.4, 139.2, 147.2, 148.4, 152.8, 159.1; MS (ES+) m/z (%) 387.2 (MH^+, 75); HRMS Calcd for $C_{20}H_{23}N_2O_6$ (MH^+): 387.1556. Found: 387.1540; Calcd for $C_{20}H_{22}N_2O_6$: C, 62.17; H, 5.74; N, 7.25. Found: C, 62.06; H, 5.75; N, 7.15.

4.1.4.9. 1,2-Dihydro-5-(2,4,5-trimethoxyphenyl)-4-(3,4-dimethoxyphenyl)pyrazol-3-one (12i). Yield: 100%; mp 203–206 °C (EtOAc); IR (KBr) 3360, 1615, 1522, 1463, 1248, 1218, 1208, 1031; ^{1}H NMR (DMSO-d_6) δ 3.53 (3H, s), 3.58 (3H, s), 3.59 (3H, s), 3.69 (3H, s), 3.83 (3H, s), 6.76 (2H, m), 6.84 (3H, m), 11.00 (2H, br s); ^{13}C NMR (DMSO-d_6) δ 55.1, 55.5, 55.8, 56.0, 56.2, 98.5, 103.0, 110.8, 111.6, 111.7, 115.1, 119.8, 126.2, 136.4, 142.4, 146.4, 148.1, 150.1, 151.7, 158.2; MS (ESI) m/z 387.2 (MH^+, 100); Calcd for $C_{20}H_{22}N_2O_6$: C, 62.17; H, 5.74; N, 7.25. Found: C, 61.88; H, 5.81; N, 6.94.

4.2. Biology

4.2.1. Cell culture

Human cervical carcinoma HeLa (GIBCO, Grand Island, NY), laryngeal carcinoma HEp-2 (GIBCO), urinary bladder transitional cell carcinoma RT-112 (German Resource Culture for Biological Material, Germany; DSMZ), urinary bladder carcinoma T-24 (DSMZ), pancreatic carcinoma MIA PaCa-2 (American Type Culture Collection, Rockwille, USA; ATCC), and colorectal carcinoma SW620 (ATCC) cells were purchased from the indicated cell culture bank and cultured as a monolayer culture according to the provided instructions. Development of cisplatin-resistant CK2 cells from HEp-2 cells has been published previously.[38] All cell lines were maintained at 37 °C in a humidified atmosphere containing 5% of CO_2.

4.2.2. Cytotoxicity assay

Cytotoxic effect of pyrazolone-fused combretastatins and their precursors was determined by 3-(4,5-dimethylthiazol-2-yl)-2,5-diphenyltetrazolium bromide (MTT) assay[39] as described. Cells were seeded into 96-well tissue culture plates (2.5×10^3 cells/0.18 mL medium/well). On the next day different concentrations of new compounds were added (0.02 mL) to each well. Each concentration was tested in quadruplicate. Following 72 h incubation at 37 °C, the medium was aspirated, and 20 μg of MTT dye/0.04 mL medium/well was added. Four hours later, formazan crystals were dissolved in dimethyl sulfoxide (0.17 mL/well), the plates were mechanically agitated for 5 min and the optical density at 545 nm was determined on a microtiter plate reader (Awareness Technology Inc, Palm City, FL). Each experiment was repeated three times.

4.2.3. Tubulin polymerization assay

Inhibitory activity of newly synthesized compounds on tubulin polymerization in vitro was evaluated by tubulin polymerization assay CytoDINAMIX ScreenTM (Cytoskeleton Inc., Denver, CO) according to manufacturer's instructions. In brief, 100 μL of ice-cold 3 mg/mL HTS tubulin in G-PEM buffer plus 10% glycerol was added rapidly to wells of half-area 96-well plate containing aliquots (10 μL) of tested compounds in G-PEM. Control wells contained the same final concentration of DMSO (1%). The increase in absorbance was measured at 340 nm on a microplate reader Infinite M200 (Tecan Trading AG, Switzerland) at 37 °C every 30 s for 60 min. Because the amount of polymerized tubulin is directly proportional to the area under the curve (AUC), we used AUC to determine percent of the inhibition of tubulin polymerization. The AUC of the control wells (containing DMSO) was set as 100% polymerization.

4.2.4. Cell cycle analysis

HeLa cells were treated with **9f** or CA-4 for 24 h. Thereafter, both adherent and floating cells were collected, washed with PBS and fixed in 70% ethanol at −20 °C overnight. Fixed cells were treated with RNase A (30 μg/mL, Sigma) for 1 h at room temperature and afterwards stained with propidium iodide (16.7 μg/mL, Sigma) for 30 min in the dark. DNA content was analyzed by flow cytometry (FACSCalibur, Becton Dickinson, Mountain View, CA). Data were analyzed with ModFitLTTM program (Verity Software House Inc., Topsham, Maine). Apoptosis was evaluated by measuring the percentage of cells with hypodiploid DNA content (sub-G_1 population).

4.2.5. Immunofluorescence microscopy

Cells were cultured on degreased glass coverslips coated with poly-L-lysine, rinsed with PBS and fixed for 15 min at room temperature with 3.7% paraformaldehyde in PBS, followed by permeabilisation step for 10 min with 0.2% Triton X-100 in PBS. After blocking for 30 min with 3% BSA in PBS, cells were incubated for 1 h at room temperature with monoclonal antibody against β-tubulin (Sigma) diluted at 1:200 in PBS, rinsed in PBS and incubated for 1 h at room temperature with Cy3-conjugated secondary antibody (Jackson ImmunoResearch, Westgrove, PA) diluted 1:400 in PBS. After the final rinsing, the coverslips were stained with 100 ng/mL DAPI and inverted onto glass slides using DakoCytomation Fluorescent Mounting Medium (Dako Co., Carpinteria, CA) and observed on an Axiovert 35 epifluorescence microscope (Opton, Germany).

4.3. Computational chemistry

Compounds **9f**, **11g**, **12a**, **12b** and **12 c**, as well as combretastatin CA-4 were built in the program Insight II (http://accelrys.com/products/insight/), and for the purpose of complex formation the X-ray structure of α,β-tubulin–DAMA–colchicine complex (pdb code 1SA0, chains C and D)[40] was used.

The ligands colchicine and a stathmin-like domain were removed from the X-ray structure and selected substrates were docked into the colchicine binding site. Ligand docking was accomplished by the AUTODOCK3.05 program.[41] Grid of 0.375 Å spacing was centered at the colchicine binding site and its size was adjusted to cover the entire binding site. The configurations most similar to the position of the colchicine in the X-ray complex were selected.

The complexes between tubulin heterodimer and the ligands **9f**, **11a**, **11f**, **11g**, **12a**, **12b**, **12c**, **12f**, and CA-4 were completed by addition of all hydrogen atoms. According to the experimental conditions used for the kinetic measurements, all Asp and Glu were negatively charged and all Lys and Arg positively charged. Histidines were neutral and their protonation site (either N_δ or N_ε) was determined according to their neighborhood and probability of the H-bond formation.

For the purpose of complex simulation within the AMBER10 suit (http://ambermd.org),[42] selected ligands as well as GTP, GDP and the Mg^{2+} ion were parameterized using the gaff force field[43] and charges and missing parameters were determined using the modules Antechamber and Parmcheck.

Energy minimization and molecular dynamics (MD) simulations were performed with the SANDER modules of the AMBER10 package[42,44] using the ff03 force field[45] Simulations were performed in explicit solvent (TIP3P) using periodic boundary conditions with a truncated octahedron as a unit cell. To ensure neutrality of the systems 38 Na^+ ions were added. The long-range electrostatic interactions were evaluated using Particle–Mesh Ewald method[46] method with cutoff radius of 11 Å for calculating the real part contributions to electrostatic and van der Waals interactions. Before applying MD simulations the system was optimized. Energy minimization was accomplished in two steps with the protein atoms and the Mg^{2+} ion restrained to their initial position and water molecules and substrate free to move. The time step used during MD simulation was 1 fs. The equilibration was performed in two steps: heating and density adjustment. The heating-up MD simulations (temperature increasing from 0 to 300 K during 30 ps) were performed at constant volume with the protein backbone atoms restrained with a harmonic force of 90 kcal/(mol Å). Density was adjusted during another 30 ps of MD simulations at constant pressure (protein backbone atoms restrained to their initial position with a harmonic force of 20 kcal/(mol Å)). MD production runs were carried out at 300 K for at least 200 ps (for the most interesting complexes up to 1 ns). Temperature was controlled by Langevin dynamics with a collision frequency of 1 ps^{-1}. For the simulation details see our recent reference.[47]

In order to investigate polarity of the selected substrates and their propensity to interact either with polar or charged molecules/groups we accomplished Log *P* and Log *S* as well as the GRID[48] calculations. Log *P* and Log *S* were calculated using the WEB interface to the ALOGPS 2.1 program.[32]

Using the program GRID interaction energies between substrates and small chemical groups ('probes'): H_2O, NH_3^+, and O- were calculated at the nodes of the three regular three-dimensional grid with 1 Å spacing. The size of the grid was adjusted to extend at least 5 Å in all directions from the surface of the substrate.

Acknowledgments

The Ministry of Higher Education, Science and Technology of Slovenia and the Slovenian Research Agency (Project P1-0230-103), and the Ministry of Science, Education and Sport of the Republic of Croatia (Projects 098-0982913-2748 and 098-1191344-2860) are gratefully acknowledged for their financial support. We would like to thank Dr. Bogdan Kralj and Dr. Dušan Žigon (Mass Spectrometry Center, Jožef Stefan Institute, Ljubljana, Slovenia) for recording the mass spectra, Dr. Roko Žaja for providing help with microplate reader Infinite M200 and Mrs. Ljiljana Krajcar (Ruđer Bošković Institute, Zagreb, Croatia) for technical assistance.

Supplementary data

Supplementary data associated with this article can be found, in the online version, at doi:10.1016/j.bmc.2010.03.006.

References and notes

1. For references concerning biological activity of pyrazoles, see: Supporting Information in: Qi, X.; Ready, J. M. *Angew. Chem., Int. Ed.* **2007**, *46*, 3242.
2. Varvounis, G.; Fiamegos, Y.; Pilidis, G. *Adv. Heterocycl. Chem.* **2001**, *80*, 73.
3. Varvounis, G.; Fiamegos, Y.; Pilidis, G. *Adv. Heterocycl. Chem.* **2004**, *87*, 141.
4. Varvounis, G.; Fiamegos, Y.; Pilidis, G. *Adv. Heterocycl. Chem.* **2008**, *95*, 27.
5. Braña, M. F.; Gradillas, A.; Ovalles, A. G.; López, B.; Acero, N.; Llinares, F.; Mingarro, D. M. *Bioorg. Med. Chem.* **2006**, *14*, 9.
6. Moreau, F.; Desroy, N.; Genevard, J. M.; Vongsouthi, V.; Gerusz, V.; Le Fralliec, G.; Oliveira, C.; Floquet, S.; Denis, A.; Escaich, S.; Wolf, K.; Busemann, M.; Aschenbrenner, A. *Bioorg. Med. Chem. Lett.* **2008**, *18*, 4022.
7. Kimata, A.; Nakagawa, H.; Ohyama, R.; Fukuuchi, T.; Ohta, S.; Suzuki, T.; Miyata, N. *J. Med. Chem.* **2007**, *50*, 5053.
8. Jordan, M. A.; Wilson, L. *Nat. Rev. Cancer* **2004**, *4*, 253. and references therein.
9. See, for example: Lippert, J. W., III *Bioorg. Med. Chem.* **2007**, *15*, 605.
10. Lawrence, N. J.; Patterson, R. P.; Ooi, L.-L.; Cook, D.; Ducki, S. *Bioorg. Med. Chem. Lett.* **2006**, *16*, 5844.
11. Nam, N.-H. *Curr. Med. Chem.* **2003**, *10*, 1697. and references therein.
12. Tron, G. C.; Pirali, T.; Sorba, G.; Pagliai, F.; Busacca, S.; Genazzani, A. A. *J. Med. Chem.* **2006**, *49*, 3033. and references therein.
13. Kanthou, C.; Tozer, G. M. *Expert Opin. Ther. Targets* **2007**, *11*, 1443. and references therein.
14. Hinnen, P.; Eskens, F. A. L. M. *Br. J. Cancer* **2007**, *96*, 1159. and references therein.
15. Siemann, D. W.; Chaplin, D. J.; Walicke, P. A. *Expert Opin. Invest. Drugs* **2009**, *18*, 189. and references therein.
16. Liou, J. P.; Chang, J. Y.; Chang, C. W.; Chang, C. Y.; Mahindroo, N.; Kuo, F. M.; Hsieh, H. P. *J. Med. Chem.* **2004**, *47*, 2897.
17. Simoni, D.; Romagnoli, R.; Baruchello, R.; Rondanin, R.; Rizzi, M.; Pavani, M. G.; Alloatti, D.; Giannini, G.; Marcellini, M.; Riccioni, T.; Castorina, M.; Guglielmi, M. B.; Bucci, F.; Carminati, P.; Pisano, C. *J. Med. Chem.* **2006**, *49*, 3143.
18. Liou, J. P.; Wu, C. Y.; Hsieh, H. P.; Chang, C. Y.; Chen, C. M.; Kuo, C. C.; Chang, J. Y. *J. Med. Chem.* **2007**, *50*, 4548.
19. Avendaño, C.; Menéndez, J. C. In *Medicinal Chemistry of Anticancer Drugs*; Elsevier: Amsterdam, 2008; pp 229–249.
20. Alloatti, D.; Giannini, G.; Cabri, W.; Lustrati, I.; Marzi, M.; Ciacci, A.; Gallo, G.; Tinti, M. O.; Marcellini, M.; Riccioni, T.; Guglielmi, M. B.; Carminati, P.; Pisano, C. *J. Med. Chem.* **2008**, *51*, 2708.
21. Wang, L.; Woods, K. W.; Li, Q.; Barr, K. J.; McCroskey, R. W.; Hannick, S. M.; Gherke, L.; Credo, R. B.; Hui, Y. H.; Marsh, K.; Warner, R.; Lee, J. Y.; Zielinski-Mozng, N.; Frost, D.; Rosenberg, S. H.; Sham, H. L. *J. Med. Chem.* **2002**, *45*, 1697.
22. Tron, G. C.; Pagliai, F.; Del Grosso, E.; Genazzani, A. A.; Sorba, G. *J. Med. Chem.* **2005**, *48*, 3260.
23. Pirali, T.; Busacca, S.; Beltrami, L.; Imovilli, D.; Pagliai, F.; Miglio, G.; Massarotti, A.; Verotta, L.; Tron, G. C.; Sorba, G.; Genazzani, A. A. *J. Med. Chem.* **2006**, *49*, 5372.
24. Bellina, F.; Cauteruccio, S.; Monti, S.; Rossi, R. *Bioorg. Med. Chem. Lett.* **2006**, *16*, 5757.
25. Gurjar, M. K.; Wakharkar, R. D.; Singh, A. T.; Jaggi, M.; Borate, H. B.; Shinde, P. D.; Verma, R.; Rajendran, P.; Dutt, S.; Singh, G.; Sanna, V. K.; Singh, M. K.; Srivastava, S. K.; Mahajan, V. A.; Jadhav, V. H.; Dutta, K.; Krishnan, K.; Chaudhary, A.; Agarwal, S. K.; Mukherjee, R.; Burman, A. C. *J. Med. Chem.* **2007**, *50*, 1744.
26. Ohsumi, K.; Hatanaka, T.; Fujita, K.; Nakagawa, R.; Fukuda, Y.; Nihei, Y.; Suga, Y.; Morinaga, Y.; Akiyama, Y.; Tsuji, T. *Bioorg. Med. Chem. Lett.* **1998**, *8*, 3153.
27. LeBlanc, R.; Dickson, J.; Brown, T.; Stewart, M.; Pati, H. N.; VanDerveer, D.; Arman, H.; Harris, J.; Pennington, W.; Holt, H. L.; Lee, M., Jr. *Bioorg. Med. Chem.* **2005**, *13*, 6025.
28. Johnson, M.; Younglove, B.; Lee, L.; LeBlanc, R.; Holt, H., Jr.; Hills, P.; Mackay, H.; Brown, T.; Mooberryd, S. L.; Lee, M. *Bioorg. Med. Chem. Lett.* **2007**, *17*, 5897.
29. Burja, B.; Kočevar, M.; Polanc, S. *Tetrahedron* **2009**, *65*, 8690.
30. Gaukroger, K.; Hadfield, J. A.; Lawrence, N. J.; Nolan, S.; McGown, A. T. *Org. Biomol. Chem.* **2003**, *1*, 3033.
31. Tetko, I. V.; Tanchuk, V. Y. *J. Chem. Inf. Comput. Sci.* **2002**, *42*, 1136.
32. Tetko, I. V.; Gasteiger, J.; Todeschini, R.; Mauri, A.; Livingstone, D.; Ertl, P.; Palyulin, V. A.; Radchenko, E. V.; Zefirov, N. S.; Makarenko, A. S.; Tanchuk, V. Y.; Prokopenko, V. V. *J. Comput. Aided Mol. Des.* **2005**, *19*, 453.
33. Gaukroger, K.; Hadfield, J. A.; Hepworth, L. A.; Lawrence, N. J.; McGown, A. T. *J. Org. Chem.* **2001**, *66*, 8135.
34. Tao, C.; Wang, Q.; Tapas, D.; Dasei, N. P.; Soon-Shiong, P. PCT Int. Appl. WO 059118, 2007; *Chem. Abstr.* **2007**, *147*, 9715.

35. Borrel, C.; Thoret, S.; Cachet, X.; Guénard, D.; Tillequin, F.; Koch, M.; Michel, S. *Bioorg. Med. Chem.* **2005**, *13*, 3853.
36. Ohsumi, K.; Nakagawa, R.; Fukuda, Y.; Hatanaka, T.; Morinaga, Y.; Nihei, Y.; Ohishi, K.; Suga, Y.; Akiyama, Y.; Tsuji, T. *J. Med. Chem.* **1998**, *41*, 3022.
37. Anjaneyulu, A. S. R.; Sudharani, G.; Mallavadhani, U. V.; Murthy, Y. L. N. *Indian J. Chem., Sect B*, **1991**, *30B*, 707. *Chem. Abstr.* **1991**, *115*, 114314.
38. Osmak, M.; Beketić-Orešković, L.; Matulić, M.; Sorić, J. *Mutat. Res.* **1993**, *303*, 113.
39. Mickisch, G.; Fajta, S.; Keilhauer, G.; Schlick, E.; Tschada, R.; Alken, P. *Urol. Res.* **1990**, *18*, 131.
40. Ravelli, R. B. G.; Gigant, B.; Curmi, P. A.; Jourdain, I.; Lachkar, S.; Sobel, A.; Knossow, M. *Nature* **2004**, *428*, 198.
41. Morris, G. M.; Goodsell, D. S.; Halliday, R. S.; Huey, R.; Hart, W. E.; Belew, R. K.; Olson, A. J. *J. Comput. Chem.* **1999**, *19*, 1639.
42. Case, D. A.; Darden, T. A.; Cheatham, T. E., III; Simmerling, C. L.; Wang, J.; Duke, R. E.; Luo, R.; Crowley, M.; Walker, R. C.; Zhang, W.; Merz, K. M.; Wang, B.; Hayik, S.; Roitberg, A.; Seabra, G.; Kolossváry, I.; Wong, K. F.; Paesani, F.; Vanicek, J.; Wu, X.; Brozell, S. R.; Steinbrecher, T.; Gohlke, H.; Yang, L.; Tan, C.; Mongan, J.; Hornak, V.; Cui, G.; Mathews, D. H.; Seetin, M. G.; Sagui, C.; Babin, V.; Kollman; P. A. AMBER 10, University of California, San Francisco; 2008; http://ambermd.org.
43. Wang, J.; Wolf, R. M.; Caldwell, J. W.; Kollman, P. A.; Case, D. A. *J. Comput. Chem.* **2004**, *25*, 1157.
44. Case, D. A.; Cheatham, T. E., III; Darden, T.; Gohlke, H.; Luo, R.; Merz, K. M., Jr.; Onufriev, A.; Simmerling, C.; Wang, B.; Woods, R. *J. Comput. Chem.* **2005**, *26*, 1668.
45. Duan, Y.; Wu, C.; Chowdhury, S.; Lee, M. C.; Xiong, G.; Zhang, W.; Yang, R.; Cieplak, P.; Luo, R.; Lee, T.; Caldwell, J.; Wang, J.; Kollman, P. *J. Comput. Chem.* **2003**, *24*, 1999.
46. Kawata, M.; Nagashima, U. *Chem. Phys. Lett.* **2001**, *340*, 165.
47. Savić, B.; Tomić, S.; Magnus, V.; Gruden, K.; Barle, K.; Grenković, R.; Ludwig-Müller, J.; Salopek-Sondi, B. *Plant Cell Physiol.* **2009**, *50*, 1587.
48. Goodford, P. J. *J. Med. Chem.* **1985**, *28*, 849.